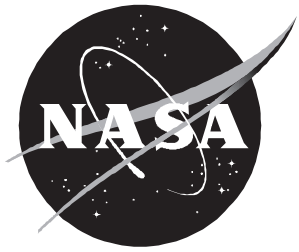

NASA Technical Memorandum 4603

Hydrogen Film Cooling With Incident and Swept-Shock Interactions in a Mach 6.4 Nitrogen Free Stream

George C. Olsen and Robert J. Nowak
Langley Research Center • Hampton, Virginia

June 1995

Available electronically at the following URL address: http://techreports.larc.nasa.gov/ltrs/ltrs.html

Printed copies available from the following:

NASA Center for AeroSpace Information
800 Elkridge Landing Road
Linthicum Heights, MD 21090-2934
(301) 621-0390

National Technical Information Service (NTIS)
5285 Port Royal Road
Springfield, VA 22161-2171
(703) 487-4650

Abstract

The effectiveness of slot film cooling of a flat plate in a Mach 6.4 flow with and without incident and swept oblique shock interactions was experimentally investigated. Hydrogen was the primary coolant gas, although some tests were conducted using helium as the coolant. Tests were conducted in the Calspan 48-Inch Shock Tunnel with a nitrogen flow field to preclude combustion of the hydrogen coolant gas. A two-dimensional highly instrumented model developed in a previous test series was used. Parameters investigated included coolant mass flow rate, coolant gas, local free-stream Reynolds number, incident oblique shock strength, and a swept oblique shock. Both gases were highly effective coolants in undisturbed flow; however, both incident and swept shocks degraded that effectiveness.

Introduction

Film cooling has been proposed as a means of thermal protection to reduce the scramjet combustor wall heating loads and the fuel mass required for regenerative cooling alone. In this concept, some of the regeneratively heated hydrogen fuel is injected at a supersonic velocity parallel to the wall through small slots to provide a buffer layer between the hot engine core flow and the structure. In addition to thermal protection, film cooling may improve engine performance by reducing skin friction and providing thrust in the high Mach number operating range. A coordinated government and industry study was conducted (refs. 1 and 2) to define film cooling technology for application to scramjet engines and to identify areas that require further data. The experimental effort reported herein is an outgrowth of this study.

Some aerothermal problems associated with hypersonic flows are summarized in reference 3. These problems include determining heat fluxes in the regions of incident-shock (two-dimensional) and swept-shock (three-dimensional) interactions with turbulent boundary layers. An oblique shock incident on a turbulent boundary layer forms a two-dimensional flow field with a separate flow region, a “lambda” shock structure (the incident and separation shock combination), and a reattachment (reflected) shock (fig. 1(a)). The interaction region becomes steady state and the extent of the separation region depends on the shock strength. An oblique shock that is swept across a turbulent boundary layer forms a three-dimensional flow field with a lambda shock and separation region structure as shown in figure 1(b) (from ref. 4). However, in the swept-shock configuration, the entire interaction region grows in a quasi-conical manner from the shock origin (ref. 4). The separated flow region becomes a spiral vortex that grows with entrained mass (fig. 1(c)). Results for a swept-shock interaction on an uncooled flat plate at similar flow conditions are reported in reference 5. These results show that heat flux and pressure rises begin 2 in. upstream and reach post-shock levels 2 in. downstream relative to inviscid shock location. Both the two-dimensional and three-dimensional flow structures are present in a scramjet combustor and are a major cause of high local heat fluxes. Film cooling is one method under consideration for reducing these fluxes. However, the addition of a coolant film in these shock and boundary-layer interactions further complicates the understanding of the fluxes.

A joint experimental two-stage program was developed by Langley Research Center (LaRC) and Calspan-University at Buffalo Research Center (CUBRC) to study film cooling for scramjet applications. The tests were conducted in the Calspan 48-Inch Shock Tunnel. (See ref. 6 for a detailed description of the test facility.) The nominal test conditions were Mach 6.4 flow at $R_\infty = 7.4 \times 10^6$/ft, $T_0 = 2189°$R, and $p_0 = 2252$ psia. Stage 1 tests (refs. 7 to 9) used helium injected at Mach 3 as the coolant gas and determined some of the fundamental phenomena that govern supersonic film cooling in a two-dimensional noncombusting environment. Parameters of the study included coolant delivery pressure, coolant slot height, lip thickness, and incident shock strength. Results for undisturbed flow were as follows:

1. Coolant pressure matched to the local boundary-layer edge pressure is most effective.

2. Larger slot heights (0.120 in.) are more effective than smaller slot heights (0.080 in.).

3. Lip thickness in the range of 0.020 to 0.205 in. has no net effect on film cooling. Data for the interactions between the film-cooling layer and the incident shock show that incident shocks degrade film-cooling effectiveness. However, these data also suggest multiple-slot film-cooling designs to reestablish the film-cooling layer downstream of a shock.

The test series reported herein, stage 2, uses hydrogen that is injected at Mach 2.7 as the primary coolant gas, although some tests with helium coolant were conducted at Mach 3. To preclude combustion when the coolant was hydrogen, the free-stream test medium for

all tests was nitrogen. The following effects were investigated:

1. Coolant mass flow rate with undisturbed flow for both hydrogen and helium coolants.
2. Incident-shock interactions for shock turning angles of 2.5°, 5.0°, and 7.5° with hydrogen coolant at a delivery pressure matched to free-stream pressure.
3. Incident-shock interactions for shock turning angles of 2.5° and 5.0° with hydrogen coolant at a delivery pressure matched to free-stream pressure and with a reduced local Reynolds number.
4. Swept-shock interactions for a shock turning angle of 5.0° with no coolant and with hydrogen coolant at delivery pressures matched to both the preshock and postshock pressures. The test matrix is shown in table I.

Symbols

c_v	specific heat, Btu/lbm-°R
g_c	acceleration due to gravity, 32.2 lbm-ft/lbf-sec^2
J	mechanical equivalent of heat, 778.16 ft-lbf/Btu
M	Mach number
m	mass flow rate, lbm/sec-in^2
p	static pressure, psia
p_0	total pressure, psia
q	heat flux, Btu/ft^2-sec
q_0	flat-plate heat flux, Btu/ft^2-sec
Q_0	Fay and Riddell heat transfer to 3-in-diameter cylinder, Btu/ft^2-sec
pos	position
R	Reynolds number at coolant slot
s	slot height, in.
T	temperature, °R
T_0	total temperature, °R
t	lip thickness, in.
V	velocity, ft/sec
x	streamwise distance from coolant slot, in.
y	transverse distance from plate centerline, in.
γ	ratio of specific heats
δ	boundary-layer thickness, in.
μ	viscosity, lbm/ft-sec
ν	kinematic viscosity, ft^2/sec

Subscripts:

c	coolant
e	boundary-layer edge
∞	free stream

Apparatus and Tests

Facility

The tests were conducted in the Calspan 48-Inch Shock Tunnel at a nominal free-stream Mach number of 6.4 with $R_\infty = 7.4 \times 10^6$/ft, $T_0 = 2189$°R, and $p_0 = 2252$ psia (table II). Nitrogen was used as the free-stream test gas to preclude combustion when hydrogen coolant gas was used. The facility and its operation and test envelope are described in reference 6. Tunnel runs had steady flow times on the order of 5 msec.

Model

The model consisted of a sharp leading-edge flat plate, a coolant distribution system with a rearward-facing coolant injection slot, instrumented downstream plates, an adjustable horizontal oblique-shock generator, and a vertical oblique-shock generator.

Configurations with 15-in-long and 28-in-long sharp-leading-edge instrumented foreplates combined with the coolant distribution section provided total leading-edge-to-coolant-slot foreplate lengths of 19 in. and 32 in., respectively. This assembly was sting mounted in the facility at zero angle of attack. Free-stream Reynolds numbers at the coolant slot locations based on length from the leading edge were 11.75×10^6 and 19.80×10^6, respectively. These Reynolds numbers provide naturally transitioned turbulent boundary layers at the coolant injection location. Analyses from the Boundary Layer Integral Matrix Procedure (BLIMP code version K, ref. 10), with a momentum integral thickness Reynolds number of 700, predicted boundary-layer thicknesses δ of 0.34 in. and 0.44 in., at the coolant slot locations.

The two-dimensional film cooling nozzles and the related coolant distribution system (fig. 2), were designed in stage 1 for uniform injection of helium at Mach 3 by using a sequential method-of-characteristics and Navier-Stokes analysis. The sequence included inviscid contour prediction, viscous analysis, contour modification for displacement thickness, and final viscous analysis. The computed helium flow was laminar with an exit boundary-layer thickness of 0.024 in. Two nozzle sets with slot heights s of 0.080 in. and 0.120 in. and a lip thickness t of 0.020 in. were fabricated. The

0.020-in. lip was considered a lower practical limit for an internally cooled structure. Forty nozzles spanned the 18-in. width of the model. The nozzles were fed, in groups of eight, from five individual high-pressure storage bottles through fast-acting valves and primary metering orifices. Coolant gas from the storage bottles entered the coolant distribution system and was channeled to the individual nozzles through equal-length flow paths and secondary metering orifices. (See fig. 2(c).) Based on stage 1 results, which show better cooling effectiveness for the larger slot height, stage 2 utilized only the 0.120-in. cooling nozzles. Adapting the nozzles for use with hydrogen coolant required the replacement of primary metering orifices in each circuit with smaller orifices to account for the difference in properties of helium and hydrogen. Repeating the original design analysis sequence for hydrogen indicated that the nozzles would still operate satisfactorily (the gas properties used in the analysis are shown in table III). Schlieren photographs (not shown) of the nozzle discharge, taken through an optical window installed in place of the instrumented plate, suggest weak internozzle wake structures and relatively uniform coolant flow. The model assembly was modified for stage 2 to incorporate O-ring seals at mating points to reduce coolant gas leakage. Coolant leakage from the lap joint (fig. 2(c)) was not totally eliminated but did not appear to be significant. The range of coolant delivery pressure (measured at the coolant nozzle exit) as a function of the boundary-layer edge pressure at the slot location p_c/p_e was 0.5 to 2.0 (with the associated mass flow rates of 0.163 to 1.580 lbm/sec-in^2). Nominal coolant flow conditions (table II) were M_c = 2.7 and $T_{0,c}$ = 536°R for hydrogen coolant and M_c = 3.0 and $T_{0,c}$ = 536°R for helium coolant.

The plates downstream of the coolant nozzles were instrumented with streamwise rows of thin-film thermometers and pressure gauges near the centerline (fig. 3). The thin-film thermometers, developed by Calspan, were platinum resistance thermometers on Corning Pyrex substrates. The thermometers were spaced 0.1 to 1.3-in. apart, with the finer spacing in the slot and shock interaction regions. Accuracy of these thin-film thermometers, including the uncertainties associated with the gauge calibration and data recording equipment, is estimated to be ±5 percent for the heating levels encountered in these tests.

Calspan-designed lead zirconium titanate piezoelectric pressure transducers capable of following fluctuations of up to 15 kHz were used to obtain mean pressure data. The frequency pressure gauges were spaced from 0.6 to 1.3 in. apart in two rows offset from the centerline (fig. 3). The system for recording the data output from the temperature and pressure instrumentation, filtering the data, and processing the data is described in reference 6.

An adjustable horizontal shock generator system (fig. 4) produced oblique shocks that were made incident on the instrumented plate 2 in. downstream of the coolant slot (based on inviscid theory). Flow turning angles of 2.5°, 5.0°, and 7.5°, with associated shock angles of 10.64°, 12.56°, and 14.70°, were investigated.

A 17-in. by 8-in. vertical shock generator was mounted on the foreplate to produce a 5° flow turning angle swept shock across the instrumented plates (fig. 5). The shock generator was translated in the *y*-direction to move the shock with respect to the lines of instrumentation. Four shock-nozzle *y*-direction crossing locations (based on inviscid theory) were tested, and the corresponding downstream location (*x*-direction) of the shock-instrumentation intersections are shown. The two lines of pressure instrumentation are offset from the centerline (fig. 3) and result in different shock crossing locations than the thin-film thermometers.

Test Procedures

Coolant injection system performance was determined in the test facility at the test static pressure (1 psia) without tunnel flow. Nozzle mass flow rates were calibrated against reservoir supply pressures. Pressure measurements that were made upstream of the primary orifice and at the nozzle plenum (downstream of the secondary orifice), throat, and exit planes during initial nozzle calibration runs indicated that the flow within the distribution system was uniform. The ratio of coolant delivery pressure to the boundary-layer edge pressure was from 0.5 to 2.0. Mass flow rates (table II) were determined from the numerical slope of the reservoir pressure versus time history over a selected period of constant flow. This method of calculating mass flow rates provided more accurate results than the method that uses the initial-to-find pressure slope (stage 1). The flow area includes lip thickness and sidewall thickness. Coolant flow conditions and mass flow rates are shown in table II. Coolant injection nozzles were sealed with aluminum tape for tests with no coolant flow to prevent backflow into the coolant distribution system.

The film-cooling tests began by initiating coolant flow in advance of tunnel flow to establish steady-state conditions in the coolant nozzles. Tunnel flow was then initiated with approximately 5 msec of steady-state flow. Thin-film thermometer and pressure data were recorded on a data acquisition system and were reduced as described in reference 6. Data reduction averaged the instrumentation output over a selected 2-msec interval of the 5-msec steady-state flow time. Heat fluxes were

determined from the thin-film thermometer data by using a semi-infinite slab approximation (ref. 6).

Reference Condition

Flat-plate (no rearward-facing step) reference conditions for heat-flux and pressure distributions over the full length of the model were established in stage 1 and are shown in figure 6. These data represent two runs, one with dense instrumentation on the foreplate and the other with dense instrumentation in the test region. A polynomial fit of the heat-flux distribution (ref. 8 and fig. 6(a)) results in the following second-order curve:

$$q(x) = 9.14 - 0.119x + 0.0034x^2 \qquad (1)$$

This heat-flux distribution is used as the reference condition for undisturbed flow cooling effectiveness results. The pressure distribution (fig. 6(b)) in the test region is uniform.

Discussion of Results

Experimentally determined heat-flux and pressure distributions downstream of the coolant injection slot are shown first in tabulated form and then as individual plots. The tabulated data have been normalized to the undisturbed flow case with no coolant by using the Fay and Riddell heat transfer to a 3-in-diameter cylinder and stagnation pressure ratios as shown in table I. The smoothed curve was computed by averaging each data point with the linear interpolation of the value from its two nearest neighbors. This smoothing, at the risk of attenuating real local maximum and minimum values of the data, removes some of the data scatter that is inherent in the flow-field nonuniformity. These smoothed curves are used to facilitate direct comparison of data sets in the text. Heat-flux distributions over the foreplate for all tests show that run-to-run variations are less than ±5 percent.

Coolant Mass Flow Effects

Heat-flux and pressure distribution data for flow with no coolant and for both hydrogen and helium coolants delivered over a range of flow rates are listed in tables IV and V, respectively. The data are plotted as follows:

1. Baseline heat flux with no coolant and the pressure data are shown in figure 7.
2. Hydrogen and helium coolant heat-flux data are shown in figures 8 and 9, respectively.
3. Hydrogen and helium coolant pressure data are shown in figures 10 and 11, respectively.

Data from the flow configuration with no coolant (fig. 7) show the low heat-flux region in the separated flow region immediately downstream of the rearward-facing step followed by a peak heat flux when the flow reattaches. After reattachment, the heat flux and pressure essentially return to the flat-plate value about ten slot heights (1.2 in.) downstream; there is some oscillation as the disturbance is damped out. There are two areas with anomalies that are probably not associated with the primary phenomenon under consideration. The first occurs in the heat flux approximately 5.5 in. from the slot and may originate at the joint between the instrumented plates. This joint was initially aligned and smoothed with wax, but may be displaced during a test by a pressure differential between the top and bottom of the plate. Pressure instrumentation in this region is not sufficient to capture the disturbance. The second anomaly is a pressure rise 10 to 14 in. downstream from the slot (out of view of the tunnel window) that is probably caused by an extraneous disturbance, such as a shock, in the flow. This pressure rise plainly appears in all the pressure data and appears less distinctly in the heat-flux data.

Heat-flux data with hydrogen and helium film coolants in an undisturbed flow are compared in figures 12(a) and 12(b), respectively. These data show that the effects of imbedded shock and expansion regions that result from the various coolant delivery pressures, $0.5 \le p_c/p_e \le 2.0$, are confined to the near-slot region (i.e., $x/s < 25$, where $x = 3$ in.). Downstream of this region the reduction in heat flux is a function of the coolant mass flow rate only. A diminishing return on heat-flux reduction by increasing coolant mass flow rates is readily apparent in the data and suggests that a given coolant mass may be more effectively used by injecting through a series of small slots spaced along the downstream direction rather than a single larger slot (also noted from the stage 1 results, ref. 8).

A comparison of heat flux for both hydrogen and helium coolant gases at the same mass flow rate, 0.662 lbm/sec-in^2, is shown in figure 12(c). The data for helium coolant at this flow rate was obtained by interpolating the bracketing flow rates. The interpolated delivery pressure ratio p_c/p_e for helium is 0.81 and 2.0 for hydrogen; however, as noted previously, the effect of delivery pressure is confined to the near-slot region. The downstream region shows that for the same mass flow rate, hydrogen coolant reduced the local heat flux 10 to 20 percent more than helium coolant.

There have been several attempts (e.g., refs. 11 and 12) to develop correlations for film cooling data. The following basic correlation is used:

$$1 - q/q_0 = (x/s)\,(m_c/m_\infty)^{-.8} \qquad (2)$$

where q_0 is the flat-plate reference heating rate, m_c is coolant mass flow per unit area, and m_∞ is the free-stream mass flow per unit area. This correlation is applied to the hydrogen and helium data in figure 13(a) and collapses the data for each gas into a single curve. However, the two gases have distinctly different curves. Suggestions of other parameters to be included in the correlation are made in reference 12. A variation of the basic correlation suggested in the present study uses a ratio of the energy flux (internal energy plus kinetic energy, $(c_v T + V^2/2g_c J)\, m$) of the two streams instead of mass flux alone, as follows:

$$1 - q/q_0 = (x/s) \left\{ \frac{[c_v T_c + (V_c^2/2g_c J)]\, m_c}{[c_v T_\infty + (V_\infty^2/2g_c J)]\, m_\infty} \right\}^{-.8} \quad (3)$$

This correlation collapses the data for both coolant gases into a single curve (fig. 13(b)).

Incident Shock Effects

Heat-flux and pressure distribution data for horizontal-wedge-induced shocks with flow turning angles of 2.5°, 5.0°, and 7.5° incident on a hydrogen coolant film with a mass flow rate of 0.260 lbm/sec-in^2 (p_c/p_e = 1.0) are listed in tables VI and VII. In addition to the base free-stream Reynolds number of 19.8×10^6, based on the foreplate length to the coolant slot, data were taken at a free-stream Reynolds number of 11.75×10^6 (2.5° and 5.0° shocks only). The heat-flux and pressure data for the base Reynolds number are shown in figures 14 and 15. The heat-flux and pressure data for the reduced Reynolds number are shown in figures 16 and 17.

Heat-flux and pressure data for the base Reynolds number cases are summarized in figure 18. If the flow were inviscid, the shocks would have impinged on the plate approximately 2 in. downstream of the slot and there would have been an instantaneous jump to the post-shock conditions. However, viscous effects alone stretch the interaction region to several inches in length (ref. 7), and the presence of the cooling layer stretches it several more inches. The values of downstream heat flux for the 5.0° and 7.5° shocks are only 6 to 8 percent less than the heat flux with no coolant (ref. 7). Interaction with an expansion fan from the trailing edge of the shock generator caused the sharp drop in the 7.5° shock heat flux starting about 14 in. from the slot. Post-shock pressure levels with 5.0° and 7.5° shocks were approximately the same as for shock results with no coolant (ref. 7), but all post-shock pressures were approximately 20 percent higher than inviscid theory predictions (fig. 15).

Heat-flux and pressure data for the reduced Reynolds number (11.75×10^6) are compared with those for the base Reynolds number (19.8×10^6) in figures 19 and 20. This 40-percent reduction in Reynolds number (the result of a shortened foreplate) and its associated reduction in free-stream boundary-layer thickness from 0.44 in. to 0.34 in. had no significant effect on either the heat-flux distribution or the pressure distribution downstream of the coolant slot (except for the anomalous excursion in heat flux downstream of the interplate joint at 5 in.).

A schlieren photograph and flow-field schematic for the 5.0° incident shock at the reduced Reynolds number are shown in figure 21 and are typical of all the incident shock tests. The photograph, taken through a 16-in-diameter window, has the coolant slot approximately centered. Two coolant nozzle assembly joints ahead of the slot still leaked some hydrogen coolant, but the disturbance degenerated to a Mach wave in the free stream so that it had minimal effect on the flow. The incident shock and reflected shocks, as well as a weak shock that appears to originate from the joint between the 5-in. and 12-in. instrumented plates (corresponds to the data fluxuations previously noted), are identified. Thinning of the boundary layer by the incident shock is evident from the dark and light regions near the wall and may indicate the thickness of the hydrogen layer and mixing layer.

Swept-Shock Effects

Heat-flux and pressure distribution data for a 5°-turning-angle, vertical-wedge-induced shock sweeping across the instrumented region are listed in tables VIII and IX. The data include flow with no coolant and with hydrogen coolant films with mass flow rates of 0.260 lbm/sec-in^2 (p_c/p_e = 1.0) and 0.662 lbm/sec-in^2 (p_c/p_e = 2.0). No-coolant data are shown in figures 22 and 23; low-coolant flow-rate data are shown in figures 24 and 25; higher flow-rate data are shown in figures 26 and 27. The shock generator was located in four different spanwise positions on the plate (fig. 5), so that the shock crossed the coolant slots at different points as indicated. The thin-film temperature gauges are located near the model centerline, but pressure instrumentation is offset in two rows (fig. 3). As a result of these offsets, the pressure distributions for position 3 gauges 1 to 9 and position 4 gauges 10 to 16 correspond to the heat-flux distribution for position 2, and the pressure distribution position 4 gauges 1 to 9 correspond to the heat-flux distribution for position 3. These data form a complete set of coincident heat-flux and pressure results that are equivalent to the configuration with the shock crossing the coolant slots at the centerline (y = 0.0)

and are shown in figure 28 for each of the coolant flow conditions.

Heat-flux distributions for the swept shock with no coolant (fig. 22) are compared with the undisturbed (no-shock) no-coolant flow distributions. The point at which the shock crosses the centerline instrumentation is labeled, except for position 1, where the shock crosses the centerline ahead of the coolant slot and the entire instrumentation region is behind the shock. Heat flux begins to rise behind the shock intersection and appears to reach a maximum and then decline. The location of the maximum moves downstream as the shock crossing point moves downstream. The decline in heat flux after the maximum is reached is the result of boundary-layer interaction with the expansion fan from the trailing edge of the shock generator (fig. 5). The pressure distributions show no increase that is directly related to the shock location (fig. 23); the pressure level seems to rise behind the slot to some uniform level that depends on the shock location—the farther downstream the shock the lower the uniform pressure level. Only when the shock is in position 1 does the downstream pressure level approach the predicted inviscid pressure level (except for the previously noted extraneous pressure rise at approximately 13 in. downstream). These behaviors suggest that the spanwise pressure gradient, induced in the free stream by the swept shock, is driving a three-dimensional relief of the flow through the boundary layer that retards the heat-flux and pressure rises.

Heat-flux and pressure distributions for the 5°-flow-turning-angle, swept shock with hydrogen coolant film and m_c = 0.260 lbm/sec-in^2 (p_c/p_e = 1.0), (figs. 24 and 25), are compared with the equivalent undisturbed flow distributions and with the results of the 2.5°-incident oblique shock which, because of shock reflection, results in the same total pressure rise (Δp = 1.03 psia). The coolant delivery pressure, p_c/p_e = 1.0, is matched to the preshock free-stream pressure. Coolant flow, in both swept and incident shock configurations, reduces the heat flux in the near-slot region, $x \leq 5$ in., to nearly zero. The 5°-swept-shock heat flux rises to the undisturbed value (fig. 22) between $5 < x < 10$ in., but the 2.5°-incident-shock heat flux does not reach the undisturbed values until $x > 15$ in. The significant difference in heat flux between these two configurations with the same pressure rise can be attributed to the growth of the separated flow region and the spiral vortex formed at the base of the swept shock. Fed by the third component of velocity, a steady supply of high-temperature fluid from the free stream is transported through the boundary layer to the wall region; conversely, the coolant film is dispersed into the mainstream flow. Pressure distributions with coolant flow (fig. 25) are virtually the same as the no-coolant pressure distributions (fig. 23).

Heat-flux and pressure distributions for the swept shock with hydrogen coolant film with a mass flow rate of 0.662 lbm/sec-in^2 (p_c/p_e = 2.0) are compared with the equivalent undisturbed flow distributions in figures 26 and 27. The coolant delivery pressure, p_c/p_e = 2.0, is matched to the post-shock free-stream pressure. This higher coolant mass flow slightly extends the region of near-zero heat-flux and retards the rise to the undisturbed level. Otherwise, the performance is similar to the lower coolant mass flow rate. Again, the pressure distributions are virtually the same as the no-coolant and the low coolant mass flow-rate data.

The composite plot of coincident heat flux and pressure data at the equivalent shock location of $y = 0.0$ shows the effect of coolant delivery pressure (mass flow rate). Matching the post-shock pressure (p_c/p_e = 2.0) instead of the preshock pressure (p_c/p_e = 1.0) doubles the coolant mass flow rate but results in only a small decrease in heat flux. This diminishing return on heat-flux reduction, as shown in the section "Coolant Mass Flow Effects," suggests that multiple small slots would be a more effective arrangement for injecting a given mass flow rate of coolant gas. Also, multiple coolant slots in the presence of swept shocks aid in renewing the coolant layer downstream of the shock interaction and reduce the effect of three-dimensional flow effects.

Concluding Remarks

An experimental test program for film cooling was conducted in the Calspan 48-Inch Shock Tunnel at a free-stream Mach number of 6.4. Hydrogen was the primary coolant gas, although some helium tests were conducted. To preclude combustion effects, the test stream was nitrogen. Test configurations included coolant mass flow rate effects in undisturbed flow over a flat plate with a rearward-facing coolant injection slot, incident shock interactions, and swept-shock interactions.

Coolant mass flow rate tests show both hydrogen and helium coolant gases to be effective in reducing wall heat flux in undisturbed flow. Hydrogen was a more effective coolant than helium. However, there was a diminishing return on heat-flux reduction with increasing mass flow rate. The basic film-cooling correlation that appears in the literature and utilizes a coolant to free-stream mass flux ratio, was modified to a coolant to free-stream energy flux ratio. The modified correlation collapses the data from both coolant gases into a single curve.

Incident oblique shock interaction tests showed that hydrogen film-cooling effectiveness was essentially destroyed by an incident shock. The region between the slot and the shock was well cooled, but downstream of the shock interaction the heat flux was nearly the same as with no-coolant flow.

Swept-shock interaction tests also showed that the region between the slot and the shock was well cooled; downstream of the shock interaction, however, the heat flux was nearly the same as with no-coolant flow. However, for shocks with equal pressure rises, the swept shock produced larger interaction regions with higher heat fluxes than did incident shocks. These higher heat fluxes are attributed to the three-dimensional growth of the resulting separated flow region and spiral vortex associated with swept shocks.

NASA Langley Research Center
Hampton, VA 23681-0001
April 10, 1995

References

1. Olsen, George C.; Nowak, Robert J.; and Baker, Ned R.: Results of Government/Industry Workshop on Film Cooling for NASP Scramjet Engine Applications. *Fifth National Aero-Space Plane Technology Symposium*, Volume 6—Structures, NASP CP-5033, NASP JPO, Wright-Patterson AFB, 1988, pp. 213–227.

2. Olsen, George C.: Results of Film Cooling Studies. *Tenth National Aero-Space Plane Technology Symposium*, Volume 6—Structures, NASP CP-10063, NASP JPO, Wright-Patterson AFB, 1991, pp. 339–363.

3. Holden, M. S.: A Review of Aerothermal Problems Associated With Hypersonic Flight. AIAA-86-0267, Jan. 1986.

4. Settles, G. S.; and Dolling, D. S.: Swept Shock/Boundary-Layer Interactions—Tutorial and Update. AIAA-90-0375, Jan. 1990.

5. Holden, M. S.: Experimental Studies of Quasi-Two-Dimensional and Three-Dimensional Viscous Interaction Regions Induced by Skewed-Shock and Swept-Shock Boundary Layer Interaction. AIAA-84-1677, June 1984.

6. Holden, Michael S.; Moselle, John R.; and Lee, Jinho: *Studies of Aerothermal Loads Generated in Regions of Shock/Shock Interaction in Hypersonic Flow.* NASA CR-181893, 1991.

7. Olsen, George C.; Nowak, Robert J.; Holden, Michael S; and Baker, N. R.: Experimental Results of Slot Film Cooling Including Shock Interaction. *Seventh National Aero-Space Plane Technology Symposium*, Volume 6—Structures, NASP CP-7045, NASP JPO, Wright-Patterson AFB, 1989, pp. 269–291.

8. Olsen, George C.; Nowak, Robert J.; Holden, Michael S.; and Baker, N. R.: Experimental Results for Film Cooling in 2-D Supersonic Flow Including Coolant Delivery Pressure, Geometry, and Incident Shock Effects. AIAA-90-0605, Jan. 1990.

9. Holden, Michael S.; Rodriguez, Kathleen M.; Nowak, Robert; and Olsen, George: Experimental Studies of Shock Wave/Wall Jet Interaction in Hypersonic Flow. AIAA-90-0607, Jan. 1990.

10. Murray, Alvin L.: *Facilitation of the BLIMP Computer Code and User's Guide*. AFWAL-TR-86-3101, Vol. I, U. S. Air Force, Jan. 1987.

11. Parthasarathy, K.; and Zakkay, V.: An Experimental Investigation of Turbulent Slot Injection at Mach 6. *AIAA J.*, vol. 8, no. 7, July 1970, pp. 1302–1307.

12. Majeski, J. A.; and Weatherford, R. H.: Development of an Empirical Correlation for Film-Cooling Effectiveness. AIAA-88-2624, June 1988.

Table I. Test Matrix

[Baseline conditions: Q_0(ref) = 61.36 Btu-ft^2/sec; p_0(ref) = 2252 psia]

Configuration	Run	Coolant		Reynolds number	Shock interaction		Normalization factors	
		Type	p_c/p_e		Type	Location, in.	Q_0/Q_0(ref)	p_0/p_0(ref)
Baseline	9	None		19.8×10^6	None		1	1
Coolant mass flow	10	H_2	0.50	19.8×10^6	None		0.996	1.025
	11	H_2	1.00	19.8×10^6	None		1.001	1.042
	12	H_2	1.50	19.8×10^6	None		0.993	1.042
	13	H_2	2.00	19.8×10^6	None		0.986	1.021
	8	He	0.50	19.8×10^6	None		1.021	1.028
	7	He	1.00	19.8×10^6	None		0.992	1.001
	6	He	1.50	19.8×10^6	None		1.081	1.080
	5	He	2.00	19.8×10^6	None		1.028	1.035
Incident shock	21	H_2	1.00	19.8×10^6	2.5° incident	x = 2.0	1.044	1.114
	17	H_2	1.00	19.8×10^6	5.0° incident	x = 2.8	0.995	1.058
	19	H_2	1.00	19.8×10^6	7.5° incident	x = 2.0	1.054	1.058
	23	H_2	1.00	11.75×10^6	2.5° incident	x = 2.0	1.050	1.066
	24	H_2	1.00	11.75×10^6	5.0° incident	x = 2.0	1.065	1.107
Swept shock	33	None		19.8×10^6	5.0° swept	y = –0.424	0.989	1.054
	35	None		19.8×10^6	5.0° swept	y = 0.0	0.978	1.058
	36	None		19.8×10^6	5.0° swept	y = 0.424	1.008	1.076
	37	None		19.8×10^6	5.0° swept	y = 0.848	1.018	1.079
	32	H_2	1.00	19.8×10^6	5.0° swept	y = –0.424	1	1.058
	29	H_2	1.00	19.8×10^6	5.0° swept	y = 0.0	1.037	1.085
	25	H_2	1.00	19.8×10^6	5.0° swept	y = 0.424	1.056	1.076
	28	H_2	1.00	19.8×10^6	5.0° swept	y = 0.848	1.033	1.082
	31	H_2	2.00	19.8×10^6	5.0° swept	y = –0.424	1.025	1.060
	30	H_2	2.00	19.8×10^6	5.0° swept	y = 0.0	1.027	1.054
	26	H_2	2.00	19.8×10^6	5.0° swept	y = 0.424	1.027	1.031
	27	H_2	2.00	19.8×10^6	5.0° swept	y = 0.848	1.041	1.074

Table II. Free Stream and Coolant Flow Conditions

Flow variable	Free stream (at coolant slot)	Coolant (at slot exit)	
		Hydrogen	Helium
M	6.4	2.7	3
R	11.75 and 19.8×10^6	293*	369*
δ, in.	0.34 and 0.44	0.024	0.019
p, psia	0.93	0.046 to 1.86	0.046 to 1.86
T_0, °R	2189	536	536
T, °R	253.5	218	134
V, ft/sec	5000	7410	5000
m, lbm/sec-in^2	0.344	0.163 (p_c/p_e = 0.5)	0.520 (p_c/p_e = 0.5)
		0.260 (p_c/p_e = 1.0)	0.749 (p_c/p_e = 1.0)
		0.460 (p_c/p_e = 1.5)	1.170 (p_c/p_e = 1.5)
		0.662 (p_c/p_e = 2.0)	1.580 (p_c/p_e = 2.0)

*Based on momentum integral thickness.

Table III. Free Stream and Coolant Gas Properties

Property	Free-stream nitrogen, T = 253.5°R	Coolant gas	
		Hydrogen, T = 218°R	Helium, T = 134°R
γ*	1.4	1.4	1.67
Gas constant, ft-lbf/lbm-°R	55.16	766.5	386.1
c_v, Btu/lbm-°R	0.18	2.46	0.74
μ, lbm/ft-sec	0.63×10^{-5}	0.38×10^{-5}	1.07×10^{-5}
ν, ft^2/sec	4.53×10^{-5}	67×10^{-5}	72×10^{-5}

*Assumed constant with temperature.

Table IV. Coolant Mass Flow Effects for Heat-Flux Data

Gauge label	Distance from slot, in.	Heat flux, Btu/ft^2-sec								
		No coolant	Hydrogen coolant				Helium coolant			
			p_c/p_e = 0.5	p_c/p_e = 1.0	p_c/p_e = 1.5	p_c/p_e = 2.0	p_c/p_e = 0.5	p_c/p_e = 1.0	p_c/p_e = 1.5	p_c/p_e = 2.0
P5H1	0.41	0.00	0.05	–0.31	–0.25	0.25	–0.78	–0.17	–0.61	–0.17
P5H2	0.50	3.33	0.20	0.93	–0.13	0.66	–0.12	1.43	–0.61	1.43
P5H3	0.60	7.77	0.49	0.55	–0.94	0.27	1.13	3.13	–0.30	3.13
P5H4	0.70	11.75	–0.01	0.25	–0.12	0.50	0.79	0.47	0.02	0.47
P5H5	0.80						1.52	1.26	0.20	1.26
P5H6	0.89	10.90	–0.67	0.38	0.59	0.71	–0.26	1.69	–0.28	1.69
P5H7	0.99	10.55	–1.85	0.78	–0.49	0.52	–0.50	–0.68	–0.93	–0.68
P5H8	1.09	10.49	–1.23	0.24	0.59	1.59	0.18	0.58	0.01	0.58
P5H9	1.17	10.64	–2.22	–1.19	–0.47	–0.18	–0.75	0.50	–1.38	0.50
P5H10	1.26	8.59	–1.90	–1.93	0.10	0.06	0.57	0.63	0.90	0.63
P5H11	1.35	8.54	–1.75	–1.39	–0.40	0.14	–0.03	1.78	0.84	1.78
P5H12	1.40						–0.38	2.16	0.73	2.16
P5H13	1.48	8.85	–0.64	0.68	–0.31	1.86	–0.70	1.82	0.09	1.82
P5H15	1.67	8.43	–0.32	0.56	–0.17	0.68	–0.20	0.98	0.81	0.98
P5H16	1.76	8.07	0.75	0.00	0.38	0.95	–0.35	2.34	0.50	2.34
P5H17	1.86	9.03	0.84	–0.22	0.40	0.92	–1.78	2.29	0.59	2.29
P5H21	2.25						0.36	3.25	0.88	3.25
P5H23	2.47	8.92	1.14	0.34	0.18	0.58	0.47	1.24	0.32	1.24
P5H24	2.57	8.70	0.97	0.21	0.05	0.40	0.32	1.45	0.26	1.45
P5H25	2.67	8.77	1.27	0.67	0.37	0.94	0.82	1.47	0.48	1.47
P5H26	2.76	8.78	1.69	1.01	0.70	1.15	0.94	1.59	0.43	1.59
P5H27	2.86	8.19	1.14	0.58	0.00	0.38	0.53	1.04	0.29	1.04
P5H28	2.96	9.11	1.52	0.84	0.44	0.83	0.97	1.51	0.37	1.51
P5H29	3.05	8.41	1.32	0.79	0.16	0.67	0.82	1.37	0.37	1.37
P5H30	3.15	8.76	1.47	0.64	0.11	0.48	0.94	1.45	0.31	1.45
P5H31	3.25	9.00	1.50	0.96	0.22	0.58	0.71	1.94	0.44	1.94
P5H32	3.34	8.36	1.25	0.42	0.19	0.31	0.97	1.42	0.44	1.42
P5H33	3.49	8.20	1.67	0.91	0.54	0.58	1.31	1.89	0.67	1.89
P5H34	3.69	7.79	1.41	0.72	0.30	0.53	0.47	0.93	0.38	0.93
P5H35	3.90	7.71	1.59	1.00	–0.06	0.51	0.30	1.11	0.48	1.11
P5H36	4.10	7.89	1.96	0.88	0.74	0.94	1.52	0.08	0.66	0.08
P5H37	4.31	8.11	1.78	1.21	0.10	0.65	0.90	1.05	0.75	1.05
P5H40	4.96	8.15	1.97	1.38	0.76	0.56	1.49	0.86	0.51	0.86
P5H41	5.16	8.18	1.90	1.57	0.70	0.51	1.24	1.16	0.52	1.16
P12H1	5.48	8.53	2.89	2.44	0.98	1.09	1.44	1.61	0.55	1.61
P12H2	5.58	8.46	2.70	2.50	0.73	0.71	1.44	1.45	0.60	1.45
P12H3	5.67	7.87	2.64	1.90	1.42	0.67	1.86	1.52	1.32	1.52
P12H4	5.77	9.06	2.99	2.47	2.32	1.20	2.13	2.14	2.12	2.14
P12H6	5.97	8.24	3.14	2.11	1.28	0.81	2.08	1.54	1.02	1.54
P12H7	6.07	7.55	2.77	1.61	1.23	0.91	2.14	0.91	0.91	0.91
P12H9	6.26	7.70	2.33	1.73	0.82	0.58	1.88	1.18	0.91	1.18
P12H11	6.46	7.42	2.62	2.25	1.00	1.06		1.61	1.32	1.61
P12H13	6.64	7.32	2.90	1.93	1.20	1.27	1.84	2.03	1.36	2.03
P12H15	6.81	7.33	3.02	2.99	1.60	0.41	2.79	2.38	1.20	2.38
P12H17	6.99	7.67	2.94	2.26	1.32	0.86	2.78	2.24	1.56	2.24
P12H19	7.17	8.00	2.81	2.08	1.06	0.80	2.38	1.88	1.26	1.88
P12H21	7.63	7.74	3.02	1.97	1.10	0.80	1.68	0.96	0.84	0.96
P12H23	8.90	7.98	3.60	2.48	1.57	1.17	2.17	1.24	1.12	1.24
P12H27	11.46	8.69	3.94	2.31	1.35	1.33		1.28	0.71	1.28
P12H29	12.74	7.00	4.12	2.73	1.70	1.54	2.71	1.36	1.37	1.36
P12H30	13.38	8.56	4.89	3.21	2.20	1.63	3.28	1.61	1.59	1.61
P12H31	14.02	8.53	5.17	3.33	2.31	1.99	3.33	1.81	1.73	1.81
P12H32	14.66	8.02	4.93	3.41	2.06	1.81	3.75	1.87	1.97	1.87
P12H33	15.31	8.59	5.20	3.49	2.30	1.92	3.69	1.75	1.75	1.75
P12H34	15.95	8.28	5.60	3.74	2.43	2.10	3.80	1.84	1.85	1.84
P12H35	16.58	8.11	5.61	3.66	2.48	2.15	3.81	1.80	1.94	1.80

Table V. Coolant Mass Flow Effects for Pressure Distribution Data

Gauge label	Distance from slot, in.	Pressure, psia								
		No coolant	Hydrogen coolant				Helium coolant			
			p_c/p_e = 0.5	p_c/p_e = 1.0	p_c/p_e = 1.5	p_c/p_e = 2.0	p_c/p_e = 0.5	p_c/p_e = 1.0	p_c/p_e = 1.5	p_c/p_e = 2.0
P5P10	0.64	0.30	0.67	0.84	0.83	1.09	1.00	0.94	1.00	
P5P1	0.73	0.58	0.73	0.80	0.87	0.76	0.80	0.86	0.72	0.68
P5P12	1.15	0.70	0.91	0.94	1.03	1.02	0.92	0.96	0.95	0.93
P5P2	1.25	0.86	1.09	1.12	1.16	1.25	1.01	1.06	1.06	1.08
P5P14	1.62	0.71	0.91	0.94	1.00	1.04	0.90	0.95	0.96	1.03
P5P3	1.76	0.83	1.00	1.04	1.06	1.09	1.01	1.04	1.03	1.13
P5P16	2.18	0.81	0.97	1.01	1.06	1.09	1.00	1.04	1.03	1.12
P5P4	2.26	0.85	0.98	1.03	1.07	1.10	1.00	1.04	1.02	1.07
P5P5	2.77	0.85	0.98	1.03	1.07	1.10	1.01	1.05	1.03	1.08
P5P6	3.27	0.85	1.05	1.07	1.14	1.16	1.06	1.10	1.06	1.13
P5P8	4.27	0.97	1.13	1.15	1.21	1.24	1.14	1.17	1.14	1.22
P5P9	4.77	0.82	0.98	0.98	1.03	1.04	0.93	0.99	0.99	1.04
P12P1	5.72	0.92	0.96	1.00	1.05	1.03	0.97	1.03	1.00	1.03
P12P5	8.28	0.89	0.76	0.98	1.02	1.03	0.98	1.03	1.00	1.01
P12P7	9.56	0.93	0.94	0.98	0.98	0.99	0.98	1.03	0.94	0.98
P12P8	10.20	0.88	0.88	0.90	0.94	0.94	0.90	0.94	0.91	0.94
P12P9	10.84	0.82	0.90	0.92	0.96	0.96	0.88	0.93	0.90	0.92
P12P10	11.48	0.85	0.85	0.88	0.91	0.91	0.88	0.90	0.89	0.91
P12P11	12.12	0.88	0.89	0.89	0.92	0.92	0.91	0.93	0.90	0.92
P12P12	12.76	1.03	1.03	1.05	1.08	1.07	1.07	1.07	1.04	1.08
P12P13	13.40	1.07	1.06	1.10	1.13	1.12	1.10	1.09	1.07	1.11
P12P14	14.04	0.88	0.87	0.89	0.92	0.92	0.90	0.93	0.91	0.93
P12P15	14.68	0.87	0.86	0.87	0.89	0.89	0.87	0.90	0.88	0.90
P12P16	15.32	0.91	0.87	0.90	0.93	0.92	0.88	0.92	0.89	0.93
P12P17	15.96	0.91	0.92	0.93	0.95	0.94	0.93	0.96	0.92	0.95

Table VI. Incident-Shock Heat-Flux Data With Hydrogen Coolant at $m = 0.260$ $(p_c/p_e = 1.0)$

Gauge label	Distance from slot, in.	Heat flux, Btu/ft^2-sec					
		$R = 19.8 \times 10^6$				$R = 11.75 \times 10^6$	
		No shock	2.5° shock	5.0° shock	7.5° shock	2.5° shock	5.0° shock
P5H1	0.41	–0.31	–0.18	1.36	0.93	0.74	0.90
P5H2	0.5	0.93	–0.10	0.75	–0.84	–0.60	0.48
P5H3	0.6	0.55	–0.67	1.98	–0.34	–0.23	0.72
P5H4	0.7	0.25	0.20	–0.16	–1.12	–0.74	–2.56
P5H6	0.89	0.38	–0.18	–0.14	–0.13	–0.95	–0.92
P5H7	0.99	0.78	–0.12	–2.31	0.65	2.48	–1.59
P5H8	1.09	0.24	–0.71	–0.61	–0.18	–4.88	–2.94
P5H9	1.17	–1.19	0.50	–0.78	–0.12	0.53	–0.48
P5H10	1.26	–1.93	–2.30	–0.97	–1.17	–1.46	–0.51
P5H11	1.35	–1.39	–1.85	–1.93	–1.62	–0.59	–1.43
P5H13	1.48	0.68	–0.26	–2.55	0.77	–1.15	–1.10
P5H15	1.67	0.56	–2.08	–1.00	–2.39	–0.04	0.05
P5H16	1.76	0.00	–0.96	–0.56	–0.40	–0.31	–0.49
P5H17	1.86	–0.22	1.44	–2.54	2.57	–0.73	–2.44
P5H24	2.57	0.21	0.14	0.64	3.47	0.39	1.55
P5H25	2.67	0.67	0.54	0.52	3.12	0.51	2.54
P5H26	2.76	1.01	0.95	0.00	3.13	0.55	2.37
P5H27	2.86	0.58	1.21	0.46	3.09	1.19	2.10
P5H28	2.96	0.84	1.24	0.87	3.60	2.40	2.78
P5H29	3.05	0.79	1.53	0.56	3.55	1.70	2.96
P5H30	3.15	0.64	1.66	1.03	4.15	2.04	3.33
P5H31	3.25	0.96	1.89	0.95	4.15	2.33	4.05
P5H33	3.49	0.91	1.29	0.81	4.51	2.68	4.93
P5H34	3.69	0.72	1.67	3.14	6.65	4.13	5.72
P5H35	3.9	1.00	2.15	3.93	8.22	2.51	6.39
P5H36	4.1	0.88	2.52	4.05	9.62	2.80	6.09
P5H37	4.31	1.21	2.67	6.26	12.97		
P5H40	4.96	1.38	2.98	8.34	20.04	5.57	9.80
P5H41	5.16	1.57	3.37	8.12	22.21	5.55	11.51
P12H1	5.48	2.44	5.06	10.35	29.56	8.62	18.24
P12H2	5.58	2.50	5.64	10.85	29.78	7.77	17.69
P12H3	5.67	1.90	5.62	9.54	27.77	7.02	16.59
P12H4	5.77	2.47	6.45	11.44	30.22	7.53	17.41
P12H6	5.97	2.11	5.35	11.74	30.42	7.44	16.66
P12H7	6.07	1.61	4.69	12.94	31.54	6.33	18.49
P12H9	6.26	1.73	5.51	12.84	33.03	6.71	17.94
P12H11	6.46	2.25	6.48	13.23	36.49	7.91	20.30
P12H13	6.64	1.93	6.58	14.53	37.12	8.07	21.37
P12H17	6.99	2.26	6.84	16.52	40.31	6.38	21.35
P12H19	7.17	2.08	4.24	17.41	44.46	5.49	16.09
P12H21	7.63	1.97	7.66	17.51	46.95	3.37	15.79
P12H23	8.9	2.48	9.67	27.46	57.40	10.60	30.13
P12H27	11.46	2.31	12.01	29.55	55.61	11.07	32.13
P12H29	12.74	2.73	11.80	30.15	50.63	12.10	28.03
P12H30	13.38	3.21	13.99	34.63	57.00	13.93	30.66
P12H31	14.02	3.33	14.41	34.13	55.65	14.01	30.31
P12H32	14.66	3.41	15.35	34.13	49.65	14.37	30.15
P12H33	15.31	3.49	15.14	34.03	44.24	15.74	31.65
P12H34	15.95	3.74	15.24	34.23	37.38	15.47	28.74
P12H35	16.58	3.66	16.50	32.04	32.41	15.64	25.27

Table VII. Incident-Shock Pressure Distribution Data With Hydrogen Coolant at $m = 0.260$ ($p_c/p_e = 1.0$)

Gauge label	Distance from slot, in.	Pressure, psia					
		$R = 19.8 \times 10^6$				$R = 11.75 \times 10^6$	
		No shock	2.5° shock	5.0° shock	7.5° shock	2.5° shock	5.0° shock
P5P10	0.64	0.84	0.81	0.79	0.80	0.72	0.76
P5P1	0.73	0.80	0.95	0.83	0.88	0.74	0.78
P5P12	1.15	0.94	0.62	0.97	0.93	0.90	0.92
P5P2	1.25	1.12	1.11	1.06	1.08	1.01	1.05
P5P14	1.62	0.94	0.95	0.93	0.95	0.88	0.91
P5P3	1.76	1.04	0.94	1.06	1.08	1.01	1.03
P5P16	2.18	1.01	1.11	1.02	1.37	0.99	1.04
P5P4	2.26	1.03	1.35	1.07	1.88	1.06	1.09
P5P5	2.77	1.03	1.69	1.05	2.44	1.33	1.89
P5P6	3.27	1.07	1.82	1.02	2.61	1.85	2.55
P5P8	4.27	1.16	2.32	2.91	4.28	2.55	4.00
P5P9	4.77	0.98	1.80	2.79	4.08	2.35	3.61
P12P1	5.72	1.00	2.29	3.57	5.69	2.75	4.20
P12P3	7.00	0.99	2.16	4.14	7.22	2.40	4.79
P12P5	8.28	0.98	1.62	4.54	7.86	2.33	4.76
P12P7	9.56	0.98	2.37	4.94	8.49	2.18	4.40
P12P8	10.20	0.90	1.87	4.43	8.02	2.07	4.35
P12P9	10.84	0.92	2.27	4.70	8.09	1.96	3.82
P12P10	11.48	0.88	2.33	4.42	7.89	2.07	4.17
P12P11	12.12	0.90	2.15	4.57	7.95	2.05	4.03
P12P12	12.76	1.05	2.64	5.06	8.34	2.25	4.52
P12P13	13.40	1.09	2.80	5.04	7.99	2.37	4.53
P12P14	14.04	0.89	2.34	4.45	7.47	2.04	3.99
P12P15	14.68	0.87	2.24	4.33	6.60	1.99	3.88
P12P16	15.32	0.90	2.37	4.45	5.80	2.09	4.00
P12P17	15.96	0.93	2.38	4.32	4.67	2.15	3.92

Table VIII. Swept-Shock Heat-Flux Data

Gauge label	Distance from slot, in.	Heat flux, Btu/ft^2-sec											
		No coolant				m = 0.260 (p_c/p_e = 1.0)				m = 0.662 (p_c/p_e = 2.0)			
		Pos. 1	Pos. 2	Pos. 3	Pos. 4	Pos. 1	Pos. 2	Pos. 3	Pos. 4	Pos. 1	Pos. 2	Pos. 3	Pos. 4
P5H1	0.41					–1.49	–0.31	0.69	0.77	0.79	–2.34	0.84	0.69
P5H2	0.50					–1.11	0.14	–6.00	0.30	3.36	–1.37	–0.13	0.84
P5H3	0.60	8.36	9.98	10.38	9.80	–0.73	1.11	–4.30	3.32	5.93	3.46	–0.52	1.60
P5H4	0.70	18.42	13.69	14.62	13.64	2.86	0.34	–8.65	–3.46	–1.68	0.56	1.30	0.75
P5H5	0.80	18.94	11.34	14.92	12.42	–0.33	0.57	–8.81	–0.30	–2.58	2.77	–0.47	–0.26
P5H6	0.89	14.52	11.15	10.18	8.31	–0.23	–1.44	–8.56	0.07	1.82	–2.98	1.22	0.16
P5H7	0.99	11.78	12.91	11.89	9.26	0.87	–1.14	–7.85	–3.62	5.23	0.05	–0.29	–0.51
P5H8	1.09	12.56	11.54	10.89	9.21	0.10	–1.28	–3.22	–0.82	–1.10	–0.45	–1.73	0.66
P5H10	1.26	10.25	10.66	10.89	8.45	–0.72	–1.53	–2.45	–1.46	1.80	2.63	–0.69	0.86
P5H13	1.48	14.38	13.01	10.28	8.52	0.01	0.14	1.59	–0.59	–1.06	0.74	–1.54	–0.80
P5H15	1.67	10.68	11.34	10.06	9.44	–0.30	–0.56	3.09	–1.98	5.03	2.41	2.19	0.13
P5H16	1.76					–1.53	–0.52	2.84	–0.29	0.36	–1.65	–1.70	–0.22
P5H17	1.86	13.09	15.75	9.69	10.28	–0.55	0.04	0.93	0.59	–1.29	2.72	0.85	–1.78
P5H21	2.25	14.99	16.23	11.10	9.65								
P5H23	2.47	17.32	15.75	11.89	10.12	1.65	1.21	1.68	1.31	1.00	0.62	0.98	0.31
P5H24	2.57	17.20	15.65	12.10	10.28	2.07	1.88	1.92	1.90	1.35	1.15	1.05	0.80
P5H25	2.67	17.31	15.55	12.20	10.28	2.31	1.55	1.55	1.76	0.91	0.73	0.72	0.63
P5H26	2.76	17.48	15.45	12.40	10.49	1.79	1.23	1.27	1.40	0.38	0.43	0.22	0.33
P5H27	2.86	16.30	14.18	11.39	9.75	1.81	1.50	1.72	2.00	0.87	0.55	0.79	0.62
P5H28	2.96	18.04	15.65	13.00	11.20	2.25	2.05	2.09	2.06	1.65	0.97	1.08	0.69
P5H29	3.05	16.99	14.47	12.10	10.14	2.36	1.70	1.97	1.92	1.34	0.81	1.06	0.66
P5H30	3.15	17.89	15.26	12.70	10.49	2.42	1.89	2.07	2.11	1.47	1.07	1.12	0.69
P5H31	3.25	17.94	15.55	12.60	10.55	2.80	2.15	2.77	2.69	1.76	1.54	1.41	1.16
P5H33	3.49	17.30	15.26	12.50	10.69	1.98	1.77	2.26	2.05	0.97	1.24	0.64	1.27
P5H34	3.69	17.49	15.16	12.70	10.49	2.79	1.59	2.08	2.16	1.48	1.08	0.94	1.20
P5H35	3.90	16.94	14.87	12.30	9.28								
P5H36	4.10	17.00	15.06	12.90	9.69	3.20	2.29	2.66	2.26	1.23	1.39	0.67	0.85
P5H40	4.96	19.97	17.51	14.31	10.79	5.58	3.65	2.59	3.06	2.85	2.01	1.76	1.86
P5H41	5.16	20.00	17.51	14.31	10.59	5.83	3.92	2.97	3.68	2.91	2.27	2.10	2.48
P12H1	5.48	29.56	26.80	19.86	13.84	18.48	9.48	5.64	3.77	7.02	3.93	2.17	2.06
P12H2	5.58	33.19	24.25	19.25	13.74	18.40	10.00	6.45	4.30	7.10	4.20	2.69	2.81
P12H3	5.67	29.17	21.91	16.93	12.73	16.59	8.25	5.87	2.90	6.51	3.79	1.16	2.59
P12H4	5.77	28.93	23.67	18.35	13.84	15.71	9.08	7.19	3.02	6.19	5.88	2.90	2.74
P12H6	5.97	24.43	21.32	16.03	13.54	14.68	8.85	6.70	3.09	5.37	6.09	2.72	2.13
P12H7	6.07	24.64	22.20	16.83	13.13	18.06	11.41	7.77	4.01	5.91	5.87	3.89	2.73
P12H9	6.26	21.81	20.34	17.54	12.52	17.34	10.89	7.28	3.55	7.40	5.92	4.53	2.35
P12H11	6.46	21.15	20.05	17.74	12.62	17.82	10.58	8.31	3.53	8.26	6.90	4.41	2.73
P12H13	6.64	21.15	21.12	17.04	12.62	18.90	12.55	9.44	4.56	8.53	6.84	5.75	2.73
P12H17	6.99	21.08	21.71	15.83	13.64	19.15	12.76	8.18	5.20	8.99	7.62	2.81	1.78
P12H19	7.17	22.57	23.57	16.83	14.76	21.07	16.70	9.16	6.98	10.97	8.50	5.62	3.14
P12H21	7.63	23.64	24.94	17.54	14.66	21.36	15.04	11.51	7.33		9.06	4.49	2.09
P12H23	8.90	23.93	25.33	20.26	17.71	21.64	18.67	17.11	12.71	13.12	11.50	9.52	3.59
P12H27	11.46	19.94	22.30	21.97	20.16	18.97	20.12	21.65	17.46		15.00	14.79	9.99
P12H29	12.74	16.15	18.29	20.97	18.93	15.62	18.25	19.96	18.80	14.56	17.36	17.87	13.12
P12H30	13.38	18.30	20.24	23.99	22.60	17.53	20.64	22.39	21.59	15.17	19.72	21.36	15.41
P12H31	14.02	16.75	18.68	22.98	22.50	16.42	19.39	21.33	21.90	14.76	19.00	20.85	16.86
P12H32	14.66	16.59	18.58	22.68	23.31	16.34	19.08	20.70	22.93	14.25	17.87	20.75	18.43
P12H33	15.31	15.72	17.60	21.87	23.62	15.54	18.25	20.80	23.76	13.94	17.87	20.64	20.51
P12H34	15.95	14.70	16.53	20.36	22.70	14.81	17.21	19.54	23.04	13.74	17.15	19.62	20.30
P12H35	16.58	13.90	15.45	18.75	21.89	13.61	15.97	17.32	21.59	12.51	15.92	18.28	19.88

Table IX. Swept-Shock Pressure Distribution Data With Hydrogen Coolant

Gauge label	Distance from slot, in.	Pressure, psia											
		No coolant				m = 0.260 (p_c/p_e = 1.0)				m = 0.662 (p_c/p_e = 2.0)			
		Pos. 1	Pos. 2	Pos. 3	Pos. 4	Pos. 1	Pos. 2	Pos. 3	Pos. 4	Pos. 1	Pos. 2	Pos. 3	Pos. 4
P5P10	0.64	0.39	0.37	0.40	0.53	0.96	0.91	0.93	0.96	1.14	1.12	1.12	1.15
P5P1	0.73	0.97	0.92	1.21	1.23	1.30	1.29	1.38	1.37	1.48	1.49	1.50	1.47
P5P12	1.15	1.20	1.08	1.00	1.24	1.69	1.57	1.50	1.50	1.81	1.69	1.59	1.63
P5P2	1.25	1.34	1.29	1.40	1.48	1.74	1.68	1.69	1.68	1.77	1.67	1.66	1.69
P5P14	1.62	1.51	1.35	1.23	1.36	1.87	1.74	1.66	1.59	1.99	1.87	1.71	1.65
P5P3	1.76	1.54	1.44	1.45	1.52	1.83	1.71	1.67	1.62	1.93	1.79	1.67	1.68
P5P16	2.18	1.82	1.65	1.50	1.56	2.00	1.87	1.78	1.70	2.16	2.04	1.88	1.76
P5P4	2.26	1.65	1.54	1.53	1.55	1.88	1.78	1.68	1.64	2.01	1.90	1.75	1.71
P5P5	2.77	1.72	1.58	1.52	1.55	1.85	1.74	1.64	1.60	2.00	1.89	1.75	1.70
P5P6	3.27	1.77	1.59	1.50	1.51	1.82	1.70	1.59	1.57	2.00	1.88	1.75	1.69
P5P8	4.27	2.16	1.88	1.59	1.62	2.07	1.94	1.83	1.77	2.33	2.20	2.09	1.92
P5P9	4.77	1.72	1.53	1.29	1.24	1.69	1.53	1.47	1.42	1.83	1.75	1.66	1.57
P12P1	5.72	1.84	1.48	1.41	1.39	1.59	1.62	1.58	1.57	1.87	1.78	1.72	1.70
P12P3	7.00	1.62	1.38	1.28	1.37	1.43	1.45	1.46	1.44	1.66	1.62	1.62	1.60
P12P5	8.28	1.82	1.59	1.41	1.47	1.64	1.51	1.51	1.49	1.68	1.66	1.66	1.65
P12P7	9.56	1.83	1.64	1.50	1.47	1.78	1.55	1.44	1.46	1.66	1.56	1.57	1.58
P12P8	10.20	1.86	1.64	1.51	1.44	1.76	1.57	1.42	1.37	1.64	1.50	1.48	1.49
P12P9	10.84	1.77	1.62	1.46	1.37	1.70	1.54	1.36	1.28	1.60	1.45	1.40	1.43
P12P10	11.48	1.81	1.76	1.53	1.39	1.76	1.61	1.43	1.29	1.64	1.50	1.40	1.42
P12P11	12.12	1.83	1.82	1.64	1.42	1.81	1.65	1.51	1.31	1.70	1.59	1.44	1.43
P12P12	12.76	2.00	1.98	1.84	1.61	1.96	1.87	1.74	1.51	1.85	1.80	1.65	1.63
P12P13	13.40	2.02	2.00	1.95	1.67	2.03	2.00	1.83	1.59	1.95	1.88	1.72	1.64
P12P14	14.04	1.61	1.77	1.67	1.45	1.63	1.64	1.54	1.35	1.56	1.61	1.47	1.37
P12P15	14.68	1.49	1.67	1.64	1.42	1.50	1.59	1.51	1.32	1.44	1.55	1.45	1.31
P12P16	15.32	1.52	1.68	1.75	1.52	1.52	1.63	1.58	1.44	1.47	1.59	1.53	1.39
P12P17	15.96	1.42	1.65	1.73	1.58	1.44	1.61	1.61	1.50	1.40	1.56	1.58	1.41

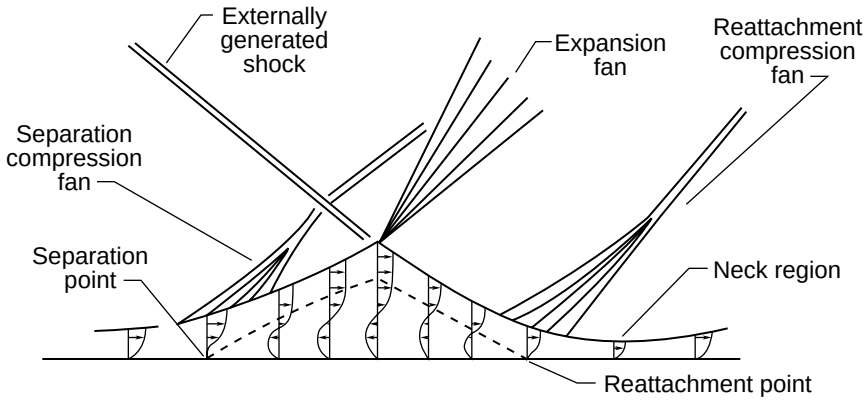

(a) Incident-shock two-dimensional flow field.

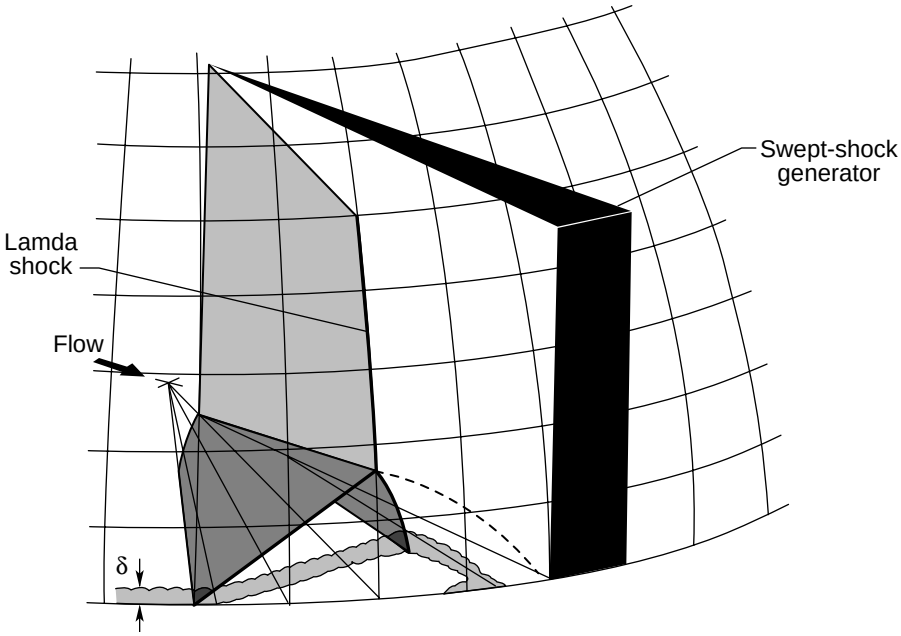

(b) Swept-shock quasi-conical interaction flow field. (From ref. 5.)

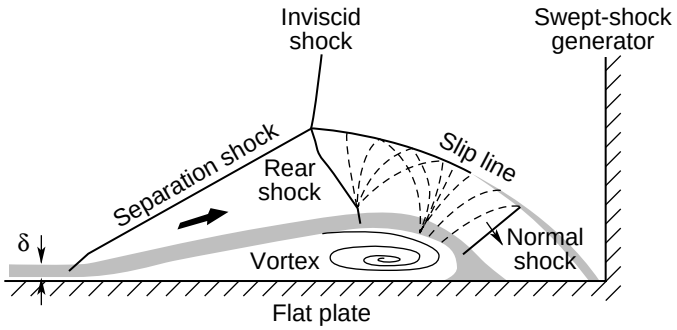

(c) Interaction flow field structure. Mach 3; $\alpha = 20°$.

Figure 1. Oblique shock and turbulent boundary-layer interactions.

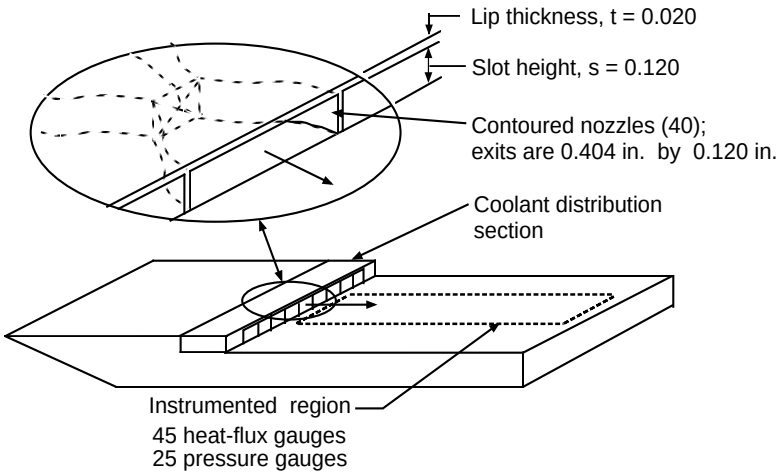

(a) Schematic of model.

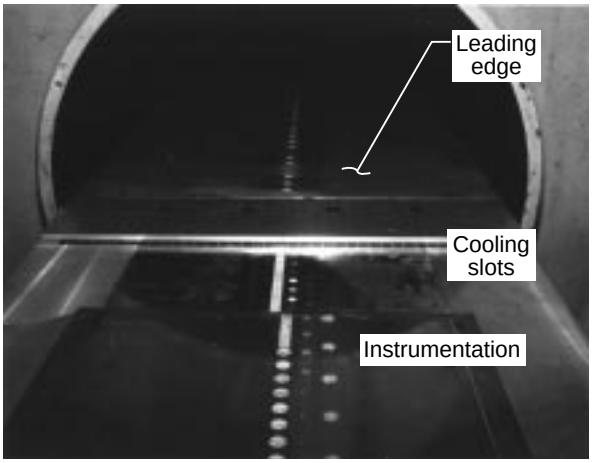

(b) Photograph of model in tunnel.

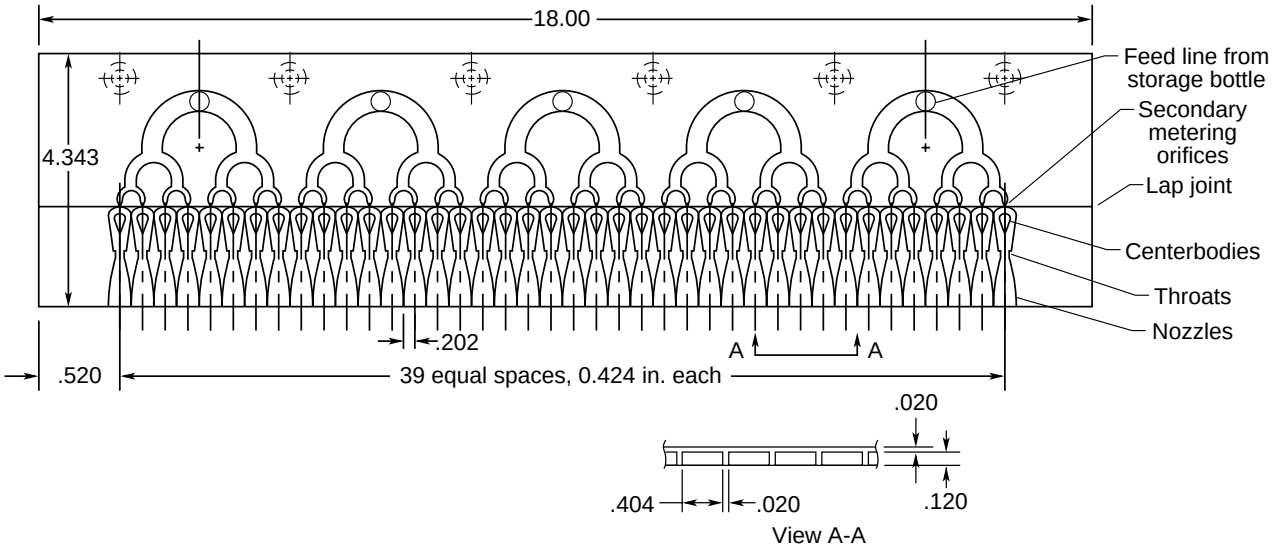

(c) Coolant distribution section.

Figure 2. Slot cooling nozzles and coolant distribution system. All dimensions are in inches.

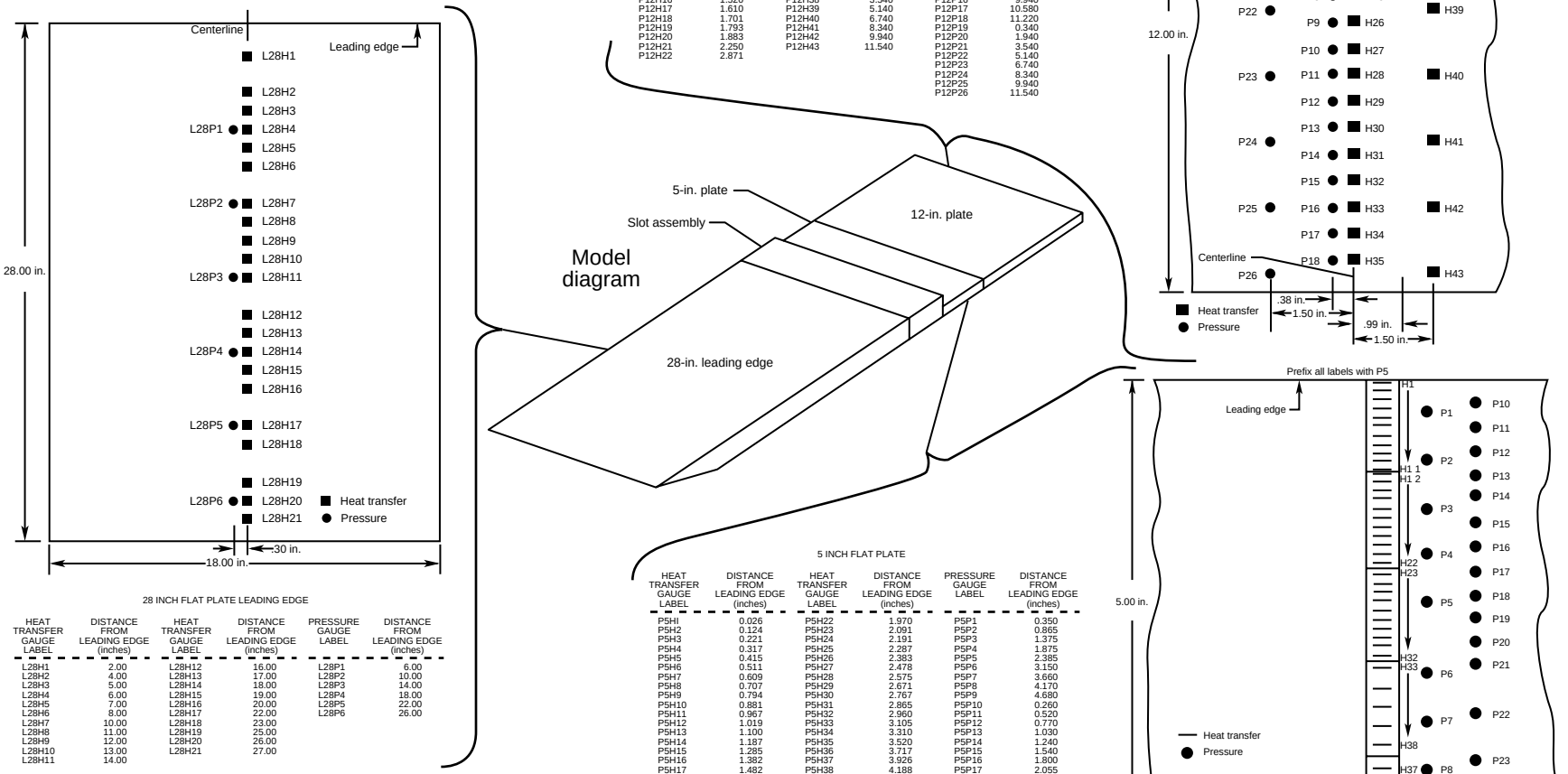

12 INCH FLAT PLATE

HEAT TRANSFER GAUGE LABEL	DISTANCE FROM LEADING EDGE (inches)	HEAT TRANSFER GAUGE LABEL	DISTANCE FROM LEADING EDGE (inches)	PRESSURE GAUGE LABEL	DISTANCE FROM LEADING EDGE (inches)
P12H1	0.103	P12H23	3.521	P12P1	0.340
P12H2	0.197	P12H24	4.167	P12P2	0.980
P12H3	0.292	P12H25	4.788	P12P3	1.620
P12H4	0.390	P12H26	5.438	P12P4	2.260
P12H5	0.490	P12H27	6.080	P12P5	2.900
P12H6	0.585	P12H28	6.716	P12P6	3.540
P12H7	0.686	P12H29	7.356	P12P7	4.180
P12H8	0.785	P12H30	7.996	P12P8	4.820
P12H9	0.883	P12H31	8.643	P12P9	5.460
P12H10	0.983	P12H32	9.283	P12P10	6.100
P12H11	1.077	P12H33	9.927	P12P11	6.740
P12H12	1.164	P12H34	10.567	P12P12	7.380
P12H13	1.257	P12H35	11.195	P12P13	8.020
P12H14	1.349	P12H36	0.340	P12P14	8.660
P12H15	1.427	P12H37	1.940	P12P15	9.300
P12H16	1.520	P12H38	3.540	P12P16	9.940
P12H17	1.610	P12H39	5.140	P12P17	10.580
P12H18	1.701	P12H40	6.740	P12P18	11.220
P12H19	1.793	P12H41	8.340	P12P19	0.340
P12H20	1.883	P12H42	9.940	P12P20	1.940
P12H21	2.250	P12H43	11.540	P12P21	3.540
P12H22	2.871			P12P22	5.140
				P12P23	6.740
				P12P24	8.340
				P12P25	9.940
				P12P26	11.540

28 INCH FLAT PLATE LEADING EDGE

HEAT TRANSFER GAUGE LABEL	DISTANCE FROM LEADING EDGE (inches)	HEAT TRANSFER GAUGE LABEL	DISTANCE FROM LEADING EDGE (inches)	PRESSURE GAUGE LABEL	DISTANCE FROM LEADING EDGE (inches)
L28H1	2.00	L28H12	16.00	L28P1	6.00
L28H2	4.00	L28H13	17.00	L28P2	10.00
L28H3	5.00	L28H14	18.00	L28P3	14.00
L28H4	6.00	L28H15	19.00	L28P4	18.00
L28H5	7.00	L28H16	20.00	L28P5	22.00
L28H6	8.00	L28H17	22.00	L28P6	26.00
L28H7	10.00	L28H18	23.00		
L28H8	11.00	L28H19	25.00		
L28H9	12.00	L28H20	26.00		
L28H10	13.00	L28H21	27.00		
L28H11	14.00				

5 INCH FLAT PLATE

HEAT TRANSFER GAUGE LABEL	DISTANCE FROM LEADING EDGE (inches)	HEAT TRANSFER GAUGE LABEL	DISTANCE FROM LEADING EDGE (inches)	PRESSURE GAUGE LABEL	DISTANCE FROM LEADING EDGE (inches)
P5H1	0.026	P5H22	1.970	P5P1	0.350
P5H2	0.124	P5H23	2.091	P5P2	0.865
P5H3	0.221	P5H24	2.191	P5P3	1.375
P5H4	0.317	P5H25	2.287	P5P4	1.875
P5H5	0.415	P5H26	2.383	P5P5	2.385
P5H6	0.511	P5H27	2.478	P5P6	3.150
P5H7	0.609	P5H28	2.575	P5P7	3.660
P5H8	0.707	P5H29	2.671	P5P8	4.170
P5H9	0.794	P5H30	2.767	P5P9	4.680
P5H10	0.881	P5H31	2.865	P5P10	0.260
P5H11	0.967	P5H32	2.960	P5P11	0.520
P5H12	1.019	P5H33	3.105	P5P12	0.770
P5H13	1.100	P5H34	3.310	P5P13	1.030
P5H14	1.187	P5H35	3.520	P5P14	1.240
P5H15	1.285	P5H36	3.717	P5P15	1.540
P5H16	1.382	P5H37	3.926	P5P16	1.800
P5H17	1.482	P5H38	4.188	P5P17	2.055
P5H18	1.579	P5H39	4.385	P5P18	2.315
P5H19	1.677	P5H40	4.584	P5P19	2.565
P5H20	1.774	P5H41	4.781	P5P20	2.820
P5H21	1.872	P5H42	4.976	P5P21	3.070
				P5P22	3.580
				P5P23	4.090
				P5P24	4.550

Figure 3. Model instrumentation layout.

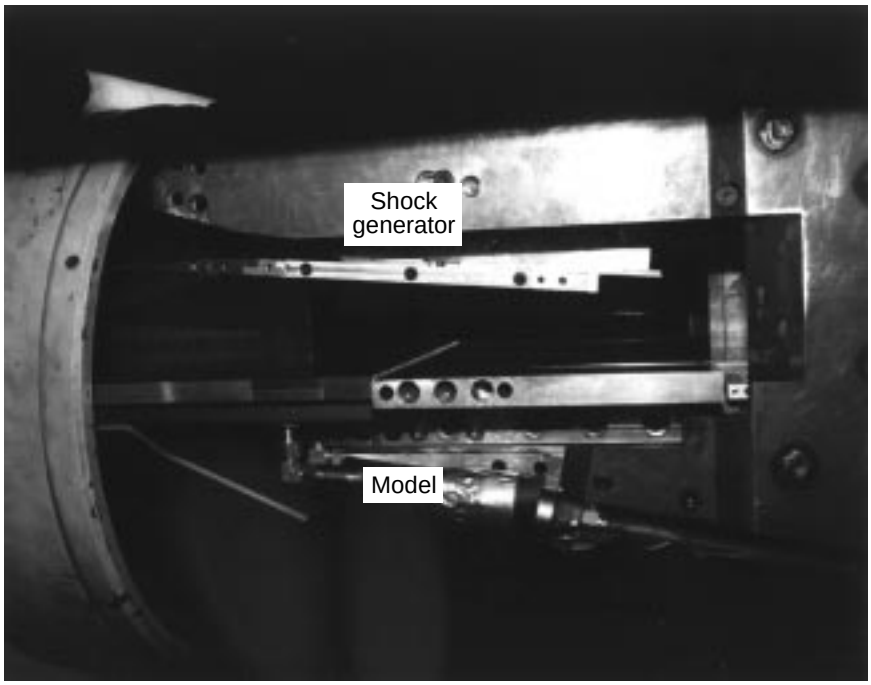

(a) Photograph.

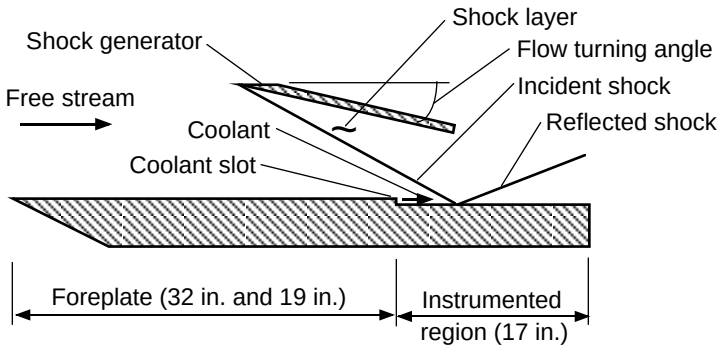

(b) Schematic.

Figure 4. Film cooling model and incident shock generator installed in Calspan 48-Inch Hypersonic Shock Tunnel.

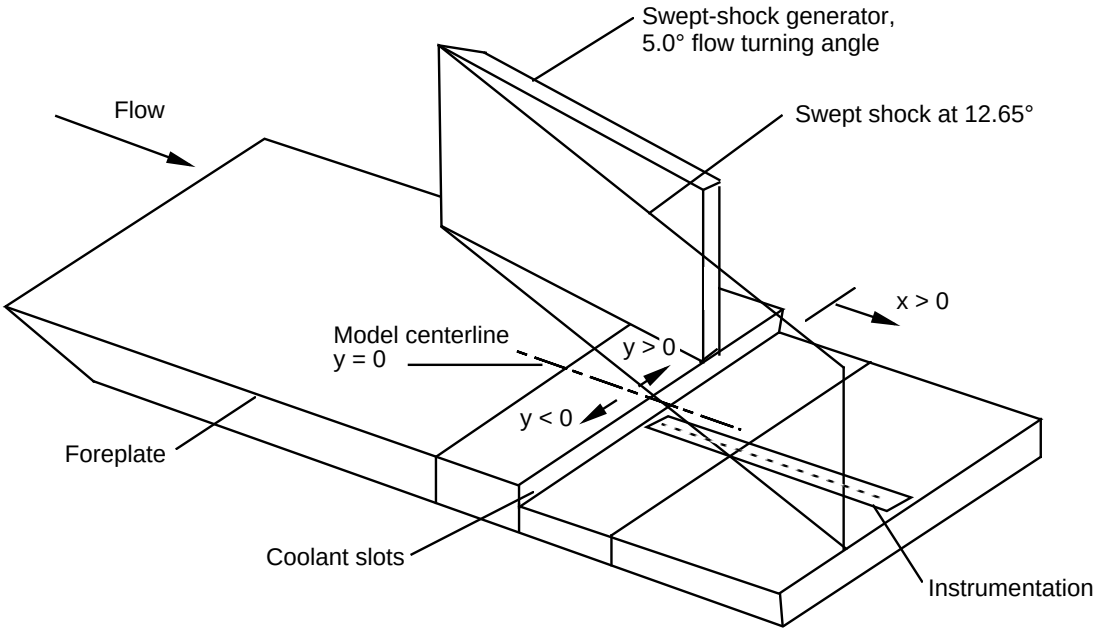

(a) Front view.

Figure 5. Film-cooling model in swept-shock configuration.

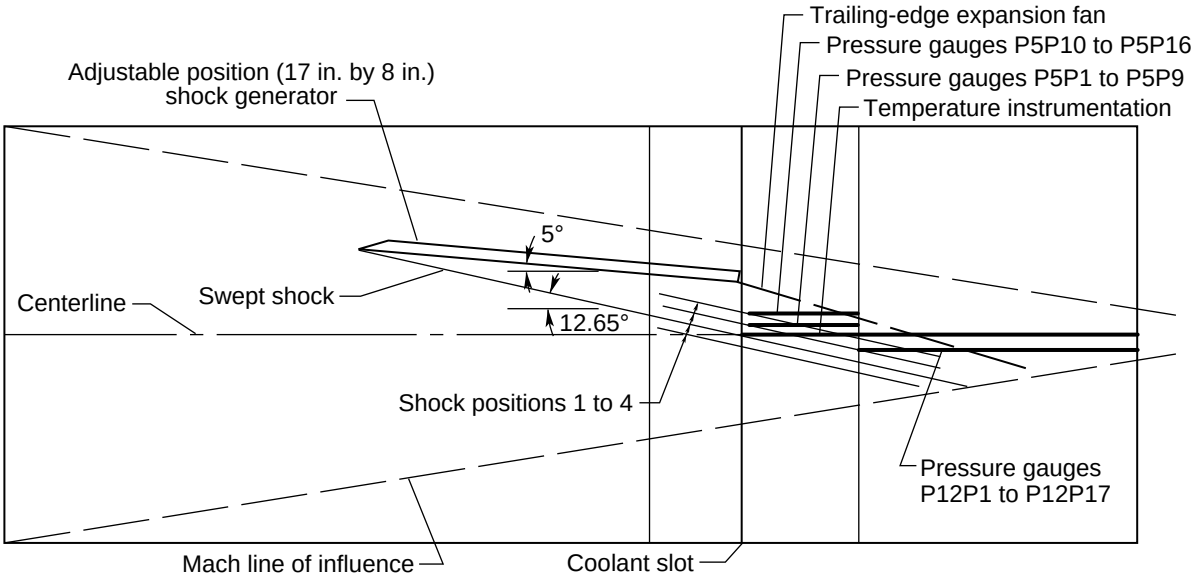

Shock-instrumentation intersections					
			Pressure instrumentation, in.		
sShock position (fig. 5(b))	Shock-slot crossing, in.	Temperature instrumentation (y = 0.0), in.	*P5P1 to P5P9 (y = 0.40 in.)	P5P10 to P5P24 (y = 0.84 in.)	P12P1 to P12P17 (y = –0.38 in.)
1	y = –0.424	x = <0	x = <0	x = <0	x = <0
2	y = 0.0	x = 0.0	x = <0	x = <0	x = 1.7
3	y = +0.424	x = 1.9	x = 0.11	x = <0	x = 3.6
4	y = +0.848	x = 3.8	x = 2.01	x = 0.0	x = 5.5

*P5P1 means 5-in. flat plate and pressure gauge 1.

(b) Plan view.

Figure 5. Concluded.

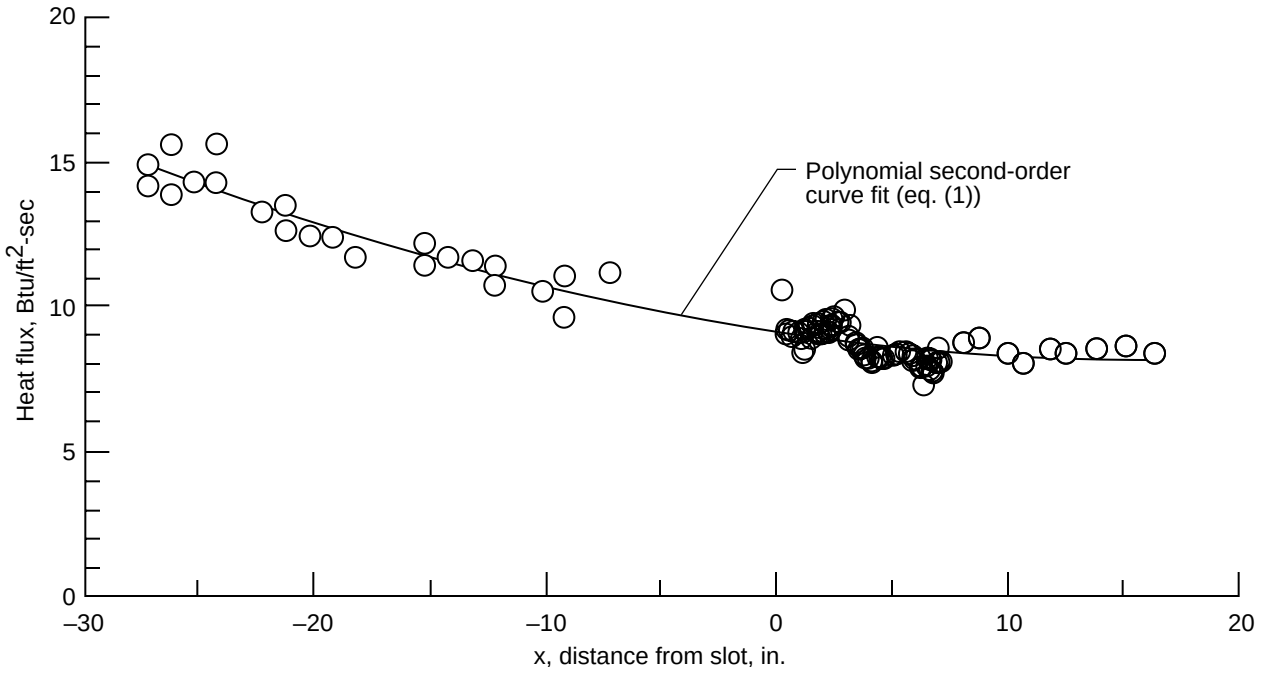

(a) Heat flux.

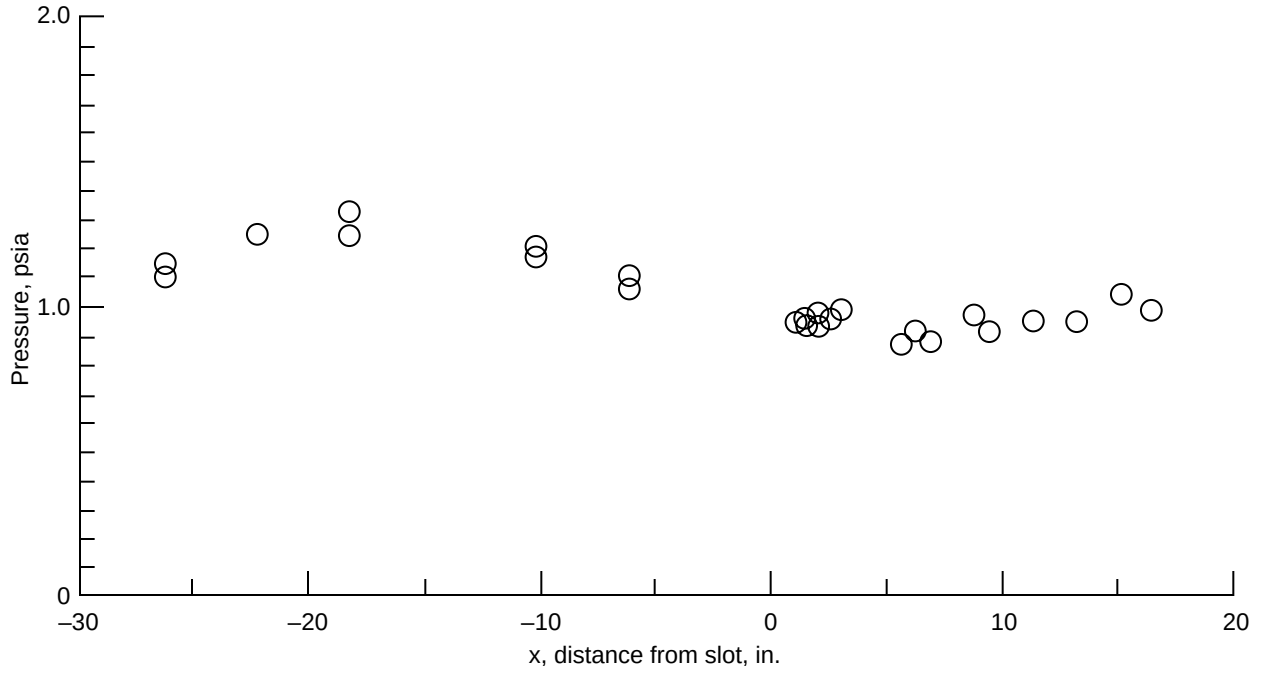

(b) Pressure.

Figure 6. Flat-plate reference conditions at $M_\infty = 6.4$, $T_0 = 2126°R$, $p_0 = 2354$ psia, and $R_\infty = 8 \times 10^6$/ft.

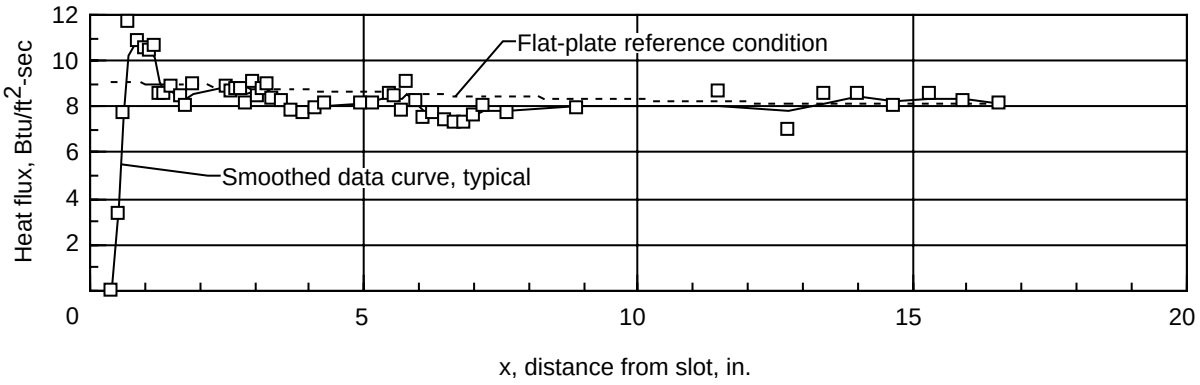

(a) Heat flux.

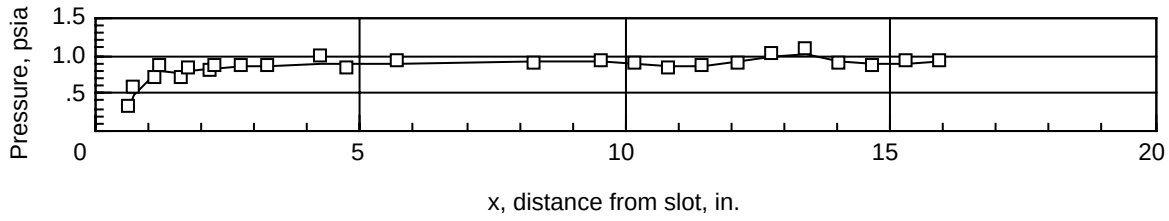

(b) Pressure.

Figure 7. Baseline configuration with no coolant.

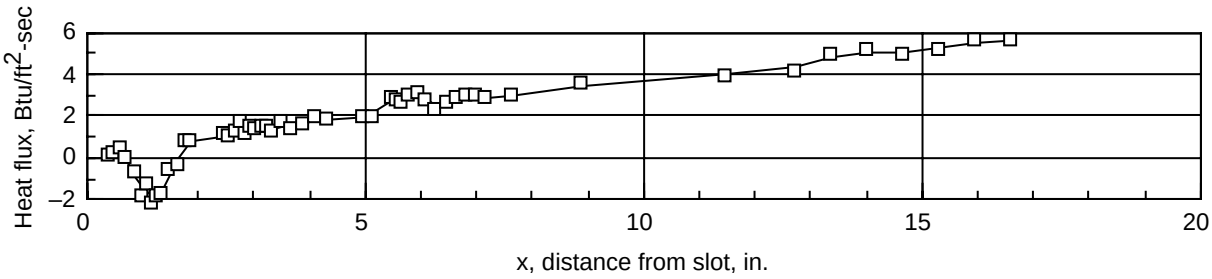

(a) m_c = 0.163 lbm/sec-in^2 (p_c/p_e = 0.5).

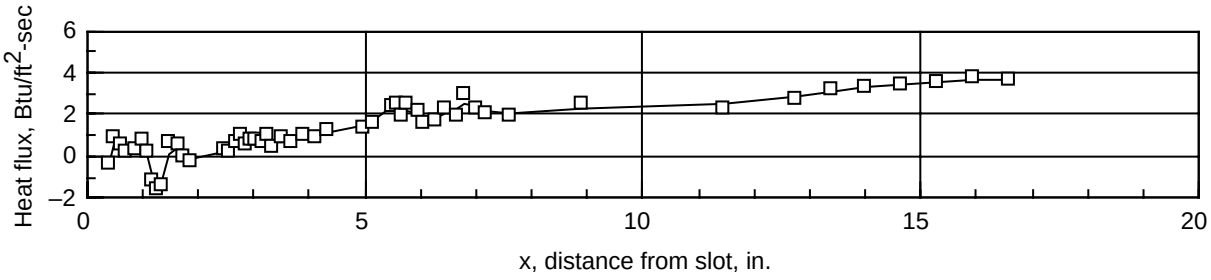

(b) m_c = 0.260 lbm/sec-in^2 (p_c/p_e = 1.0).

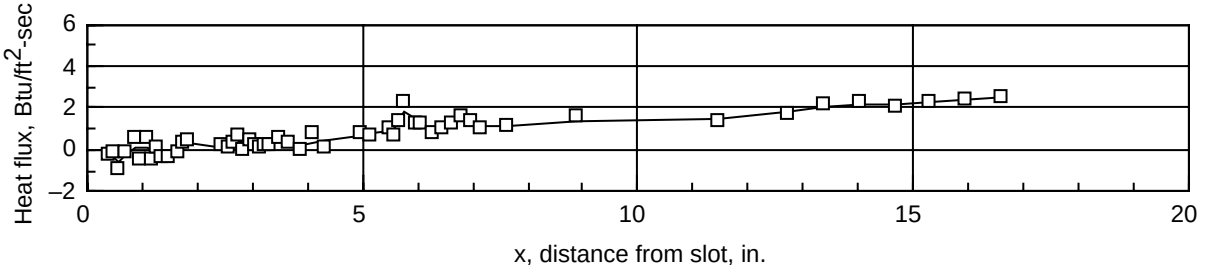

(c) m_c = 0.460 lbm/sec-in^2 (p_c/p_e = 1.5).

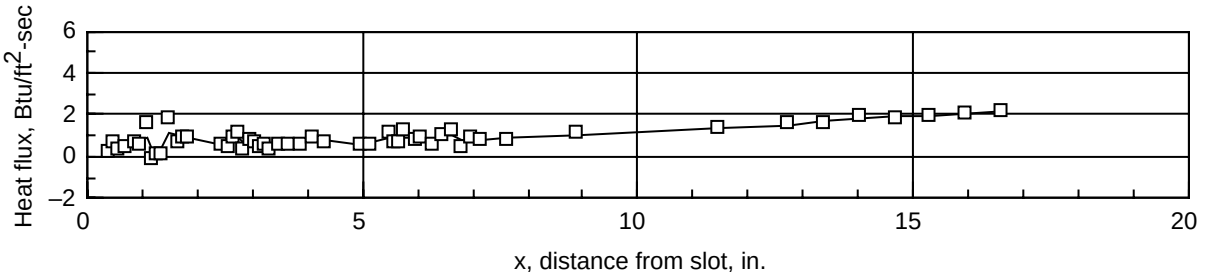

(d) m_c = 0.662 lbm/sec-in^2 (p_c/p_e = 2.0).

Figure 8. Heat-flux distributions of hydrogen film-cooling mass flow effects.

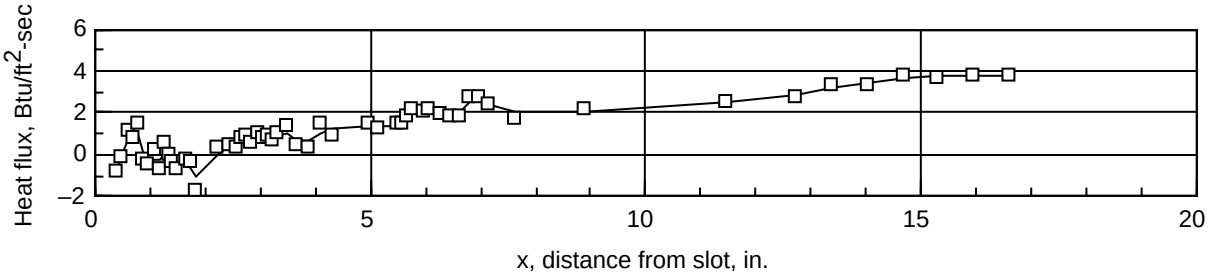

(a) m_c = 0.520 lbm/sec-in^2 (p_c/p_e = 0.5).

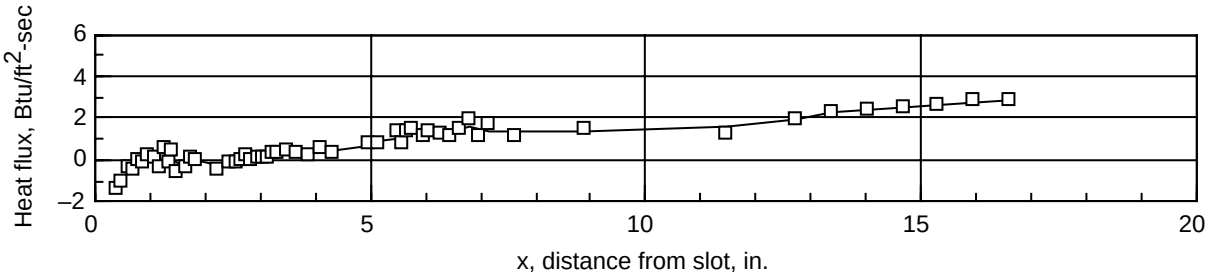

(b) m_c = 0.749 lbm/sec-in^2 (p_c/p_e = 1.0).

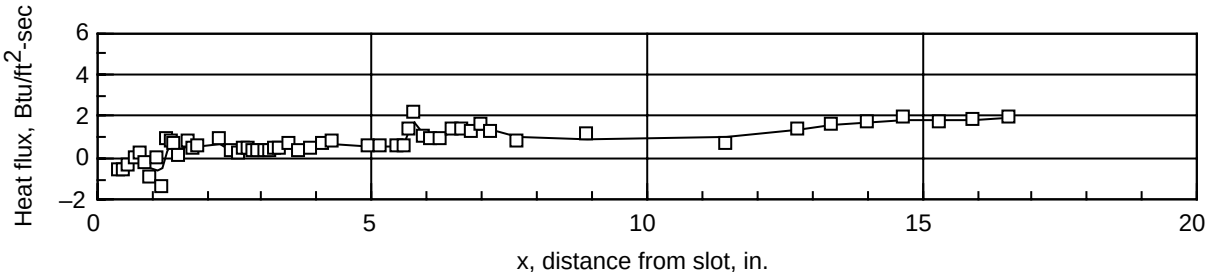

(c) m_c = 1.170 lbm/sec-in^2 (p_c/p_e = 1.5).

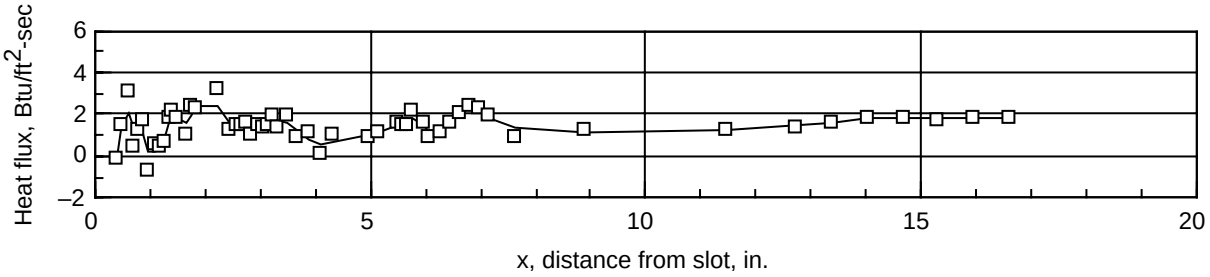

(d) m_c = 1.580 lbm/sec-in^2 (p_c/p_e = 2.0).

Figure 9. Heat-flux distributions of helium film-cooling mass flow effects.

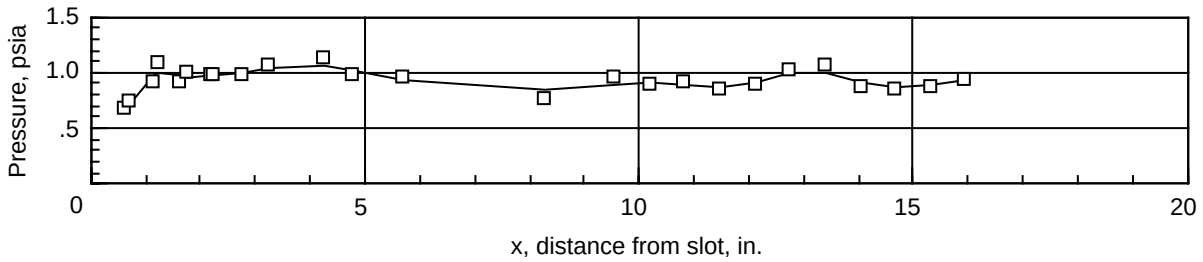

(a) m_c = 1.163 lbm/sec-in^2 (p_c/p_e = 0.5).

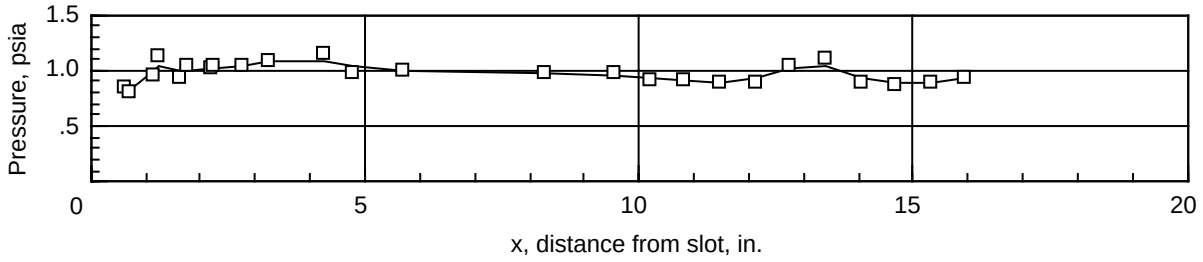

(b) m_c = 0.260 lbm/sec-in^2 (p_c/p_e = 1.0).

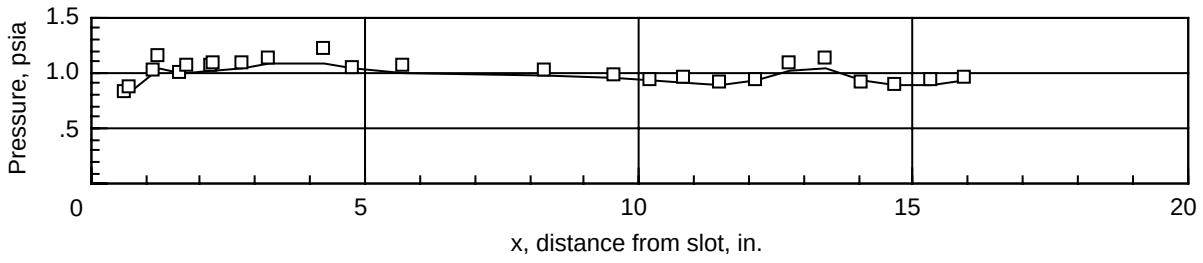

(c) m_c = 0.460 lbm/sec-in^2 (p_c/p_e = 1.5).

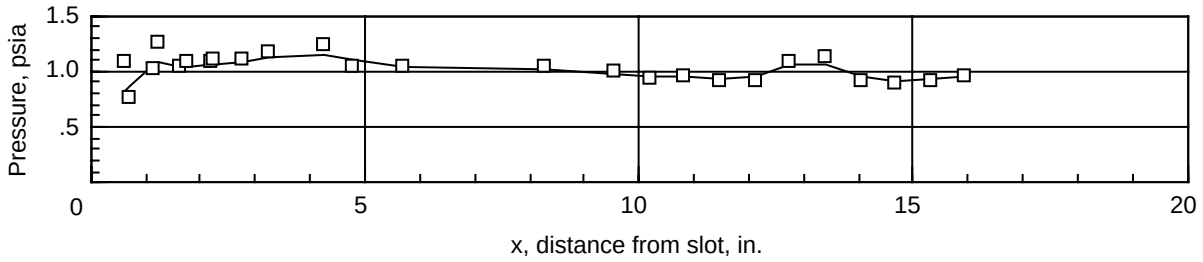

(d) m_c = 0.662 lbm/sec-in^2 (p_c/p_e = 2.0).

Figure 10. Pressure distributions of hydrogen film-cooling mass flow effects.

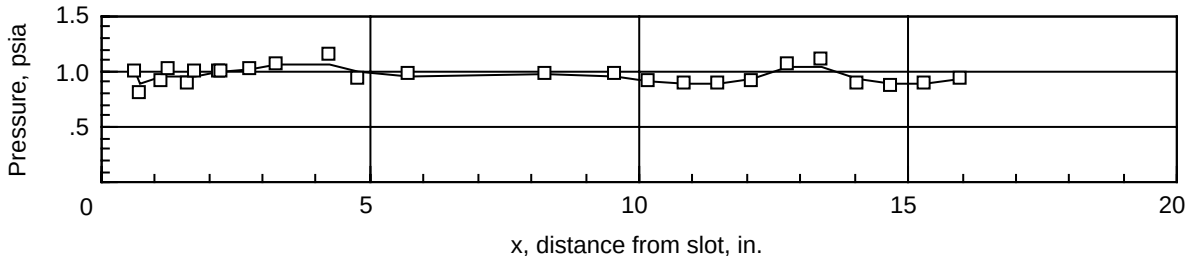

(a) m_c = 0.520 lbm/sec-in^2 (p_c/p_e = 0.5).

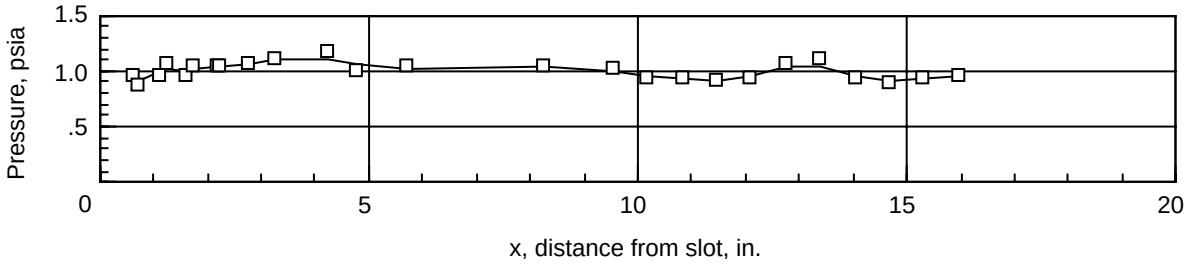

(b) m_c = 0.749 lbm/sec-in^2 (p_c/p_e = 1.0).

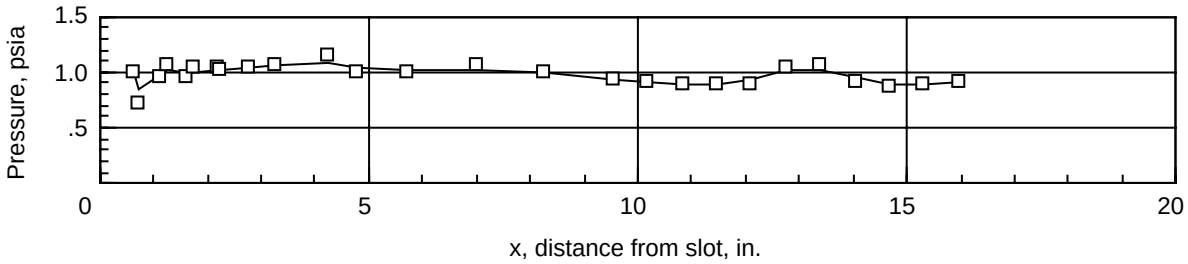

(c) m_c = 1.170 lbm/sec-in^2 (p_c/p_e = 1.5).

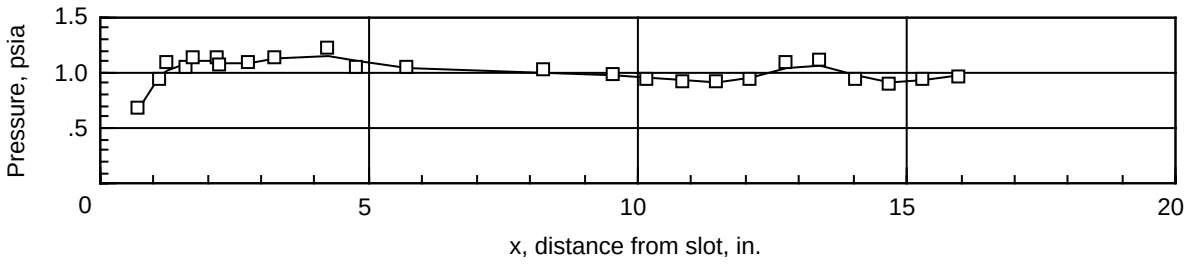

(d) m_c = 1.580 lbm/sec-in^2 (p_c/p_e = 2.0).

Figure 11. Pressure distributions of helium film-cooling mass flow effects.

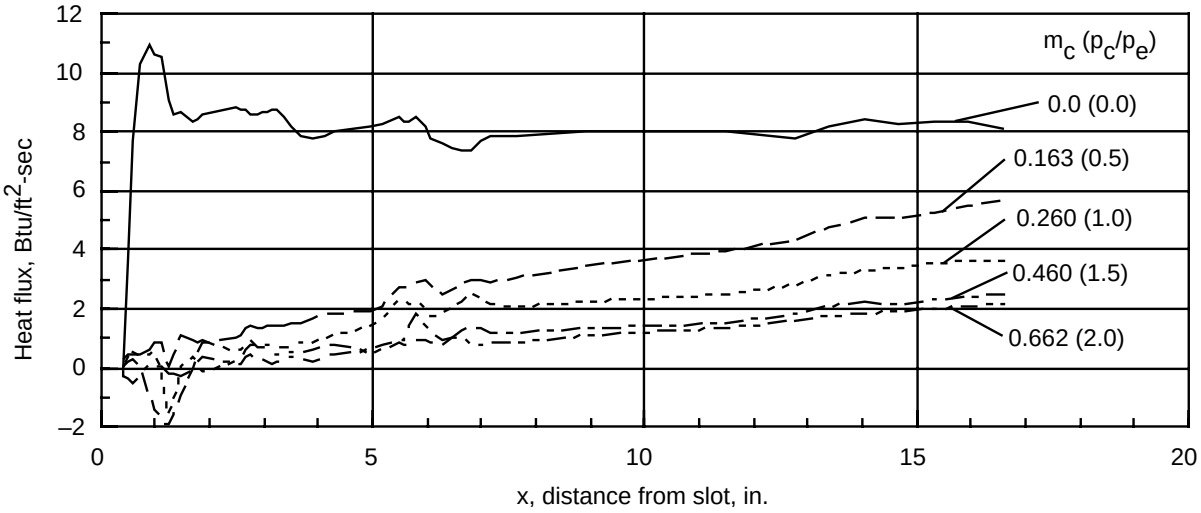

(a) Hydrogen coolant.

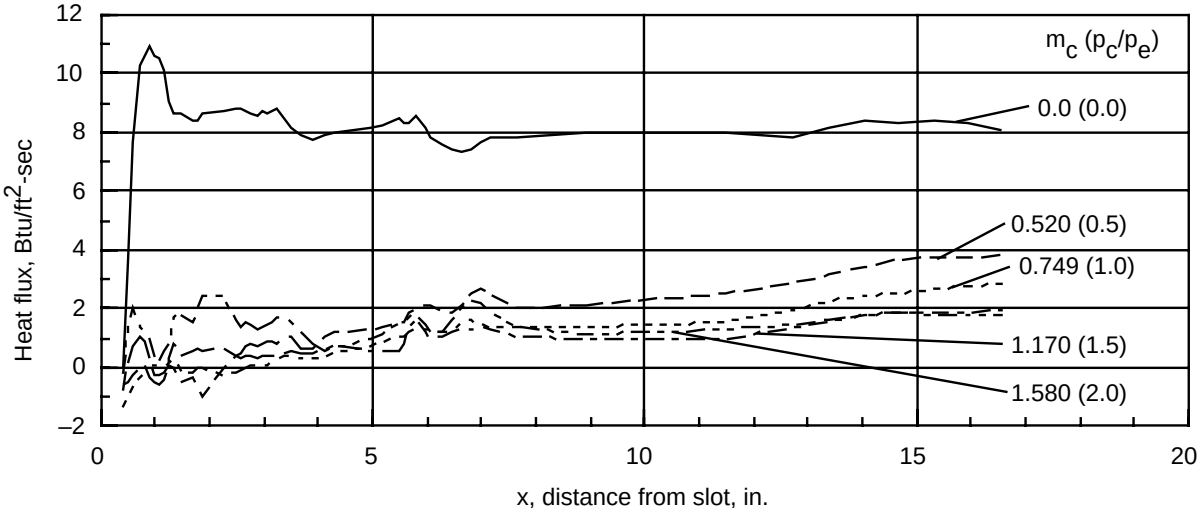

(b) Helium coolant.

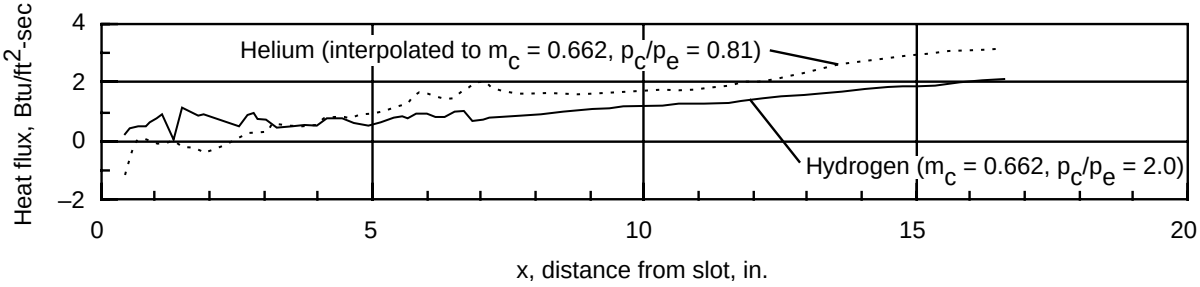

(c) Hydrogen and helium coolants at same mass flow rate.

Figure 12. Coolant mass flow effects on heat flux.

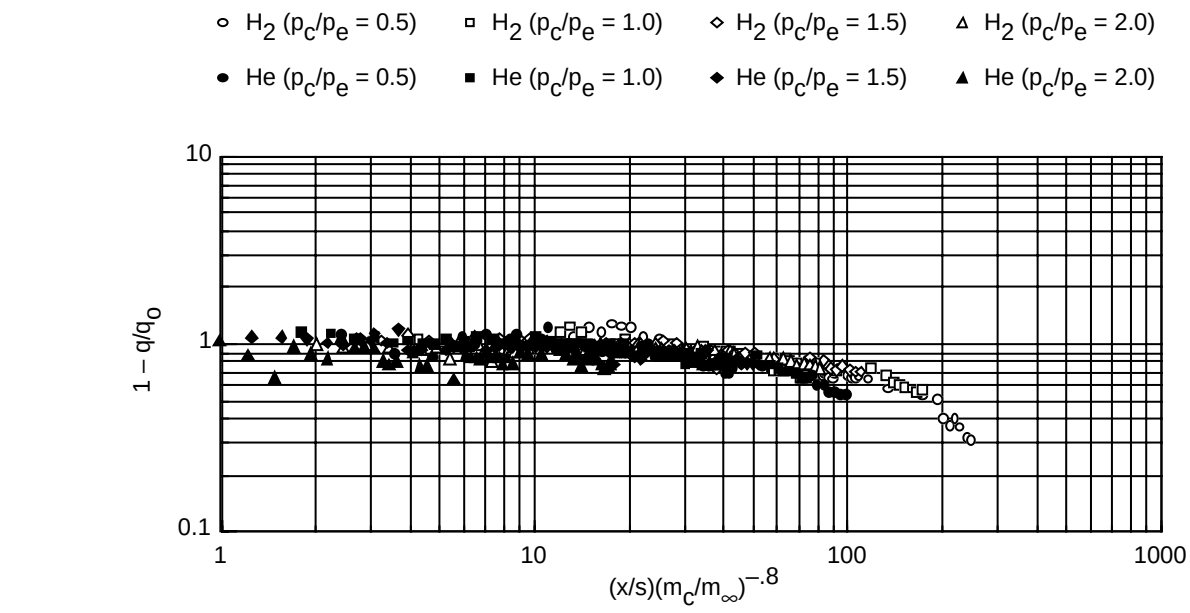

(a) Basic correlation.

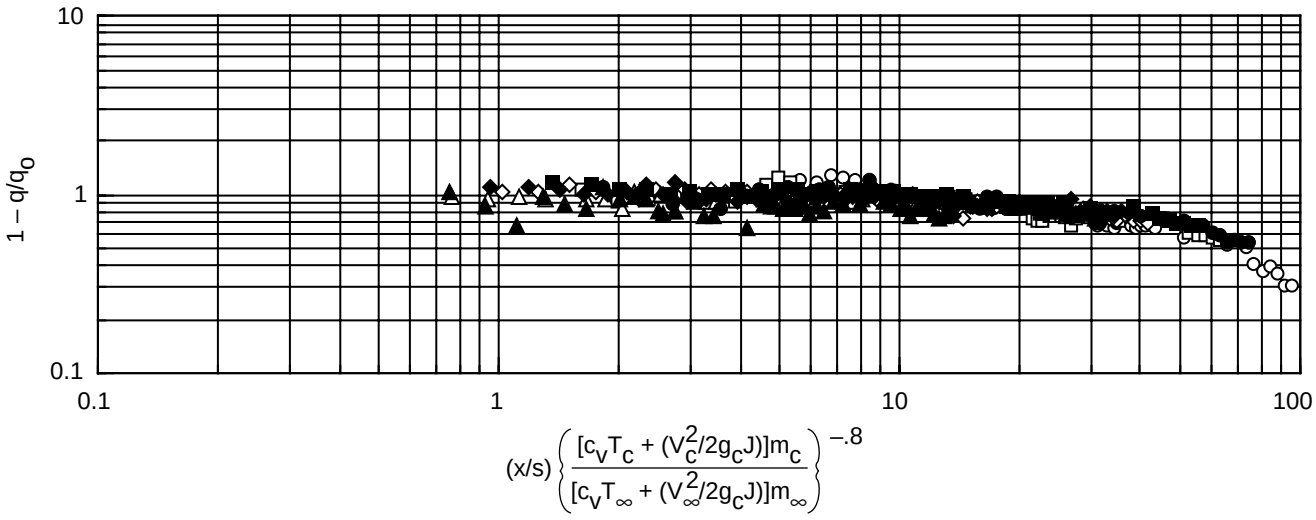

(b) Improved correlation.

Figure 13. Film-cooling correlations.

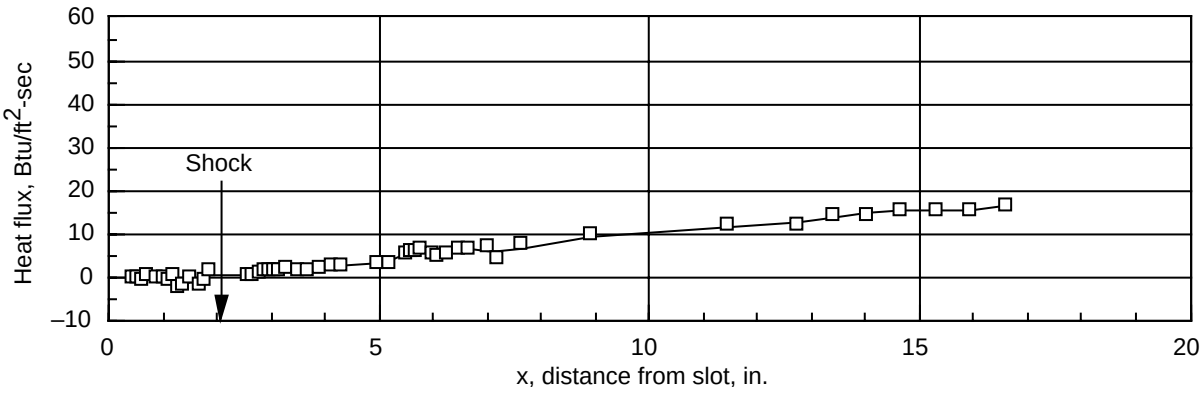

(a) 2.5° incident shock.

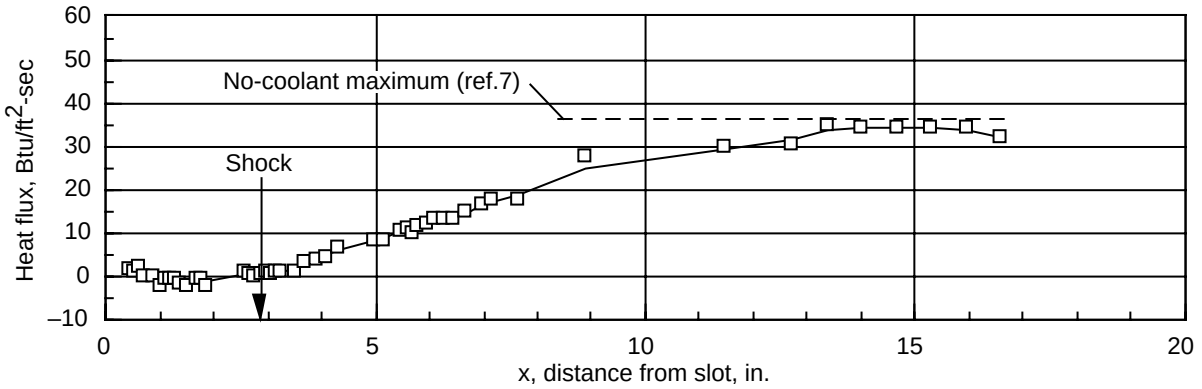

(b) 5.0° incident shock.

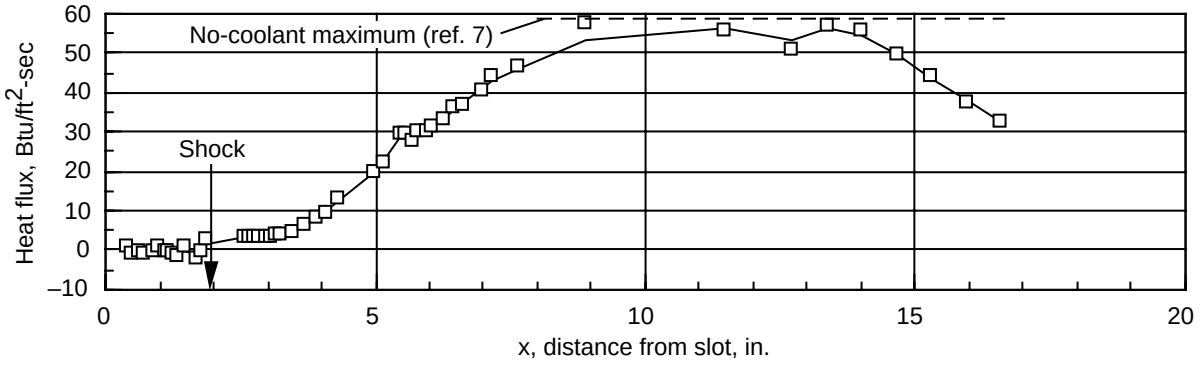

(c) 7.5° incident shock.

Figure 14. Incident-shock heat-flux distributions with hydrogen coolant at $m_c = 0.260$ ($p_c/p_e = 1.0$) and $R = 19.8 \times 10^6$.

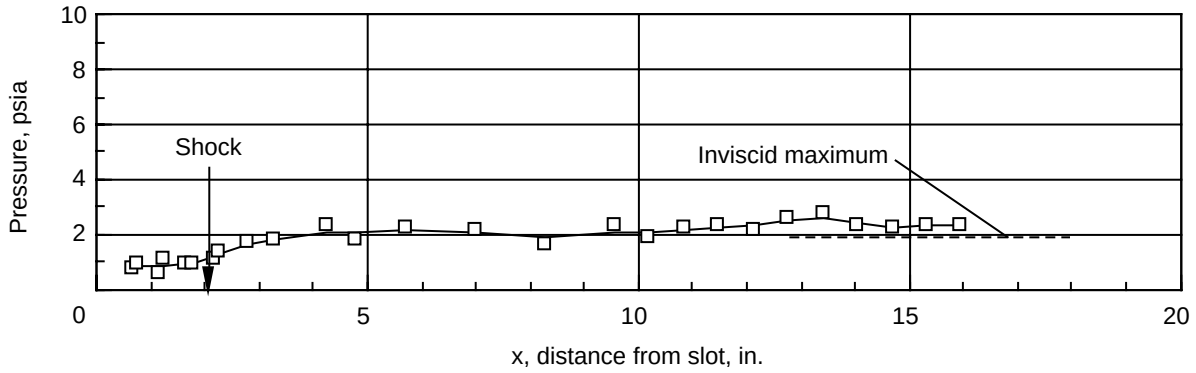

(a) 2.5° turning angle shock.

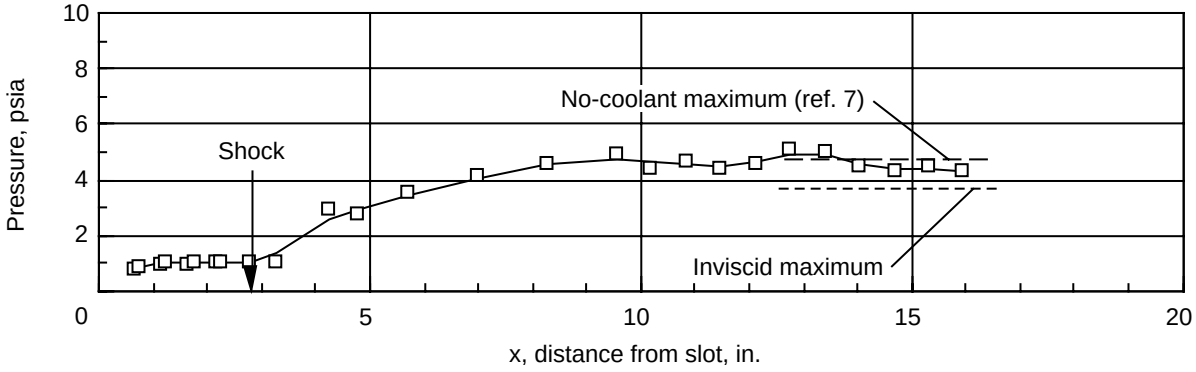

(b) 5.0° turning angle shock.

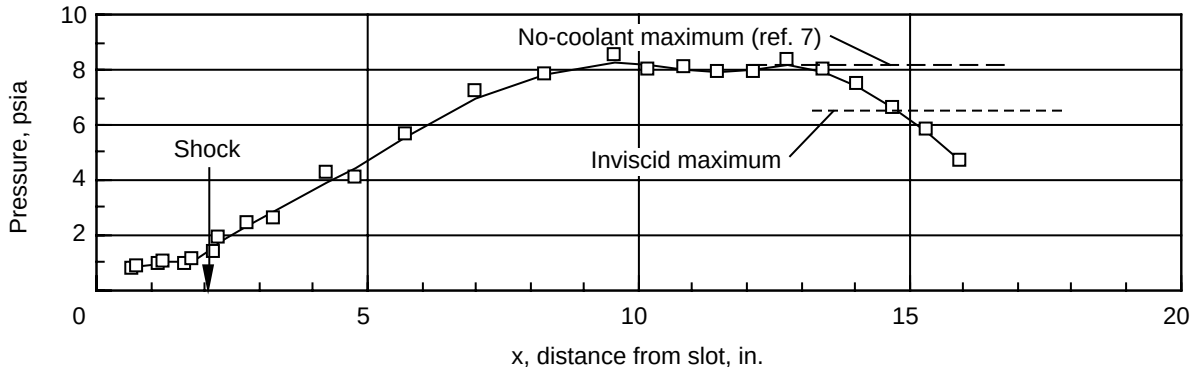

(c) 7.5° turning angle shock.

Figure 15. Incident-shock strength pressure distributions with hydrogen coolant at $m_c = 0.260$ ($p_c/p_e = 1.0$) and $R = 19.8 \times 10^6$.

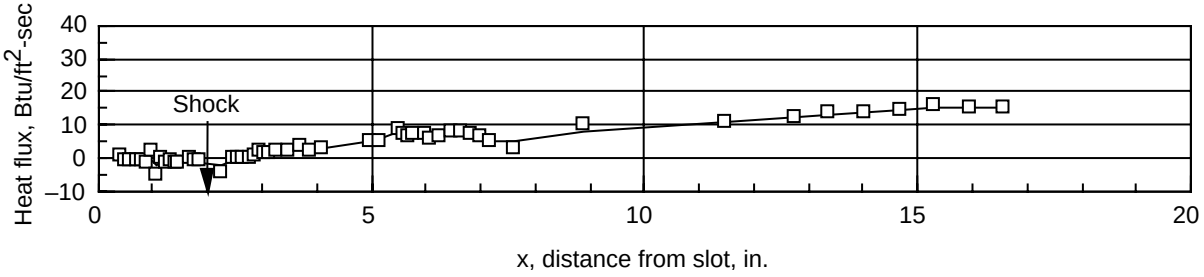

(a) 2.5° turning angle shock.

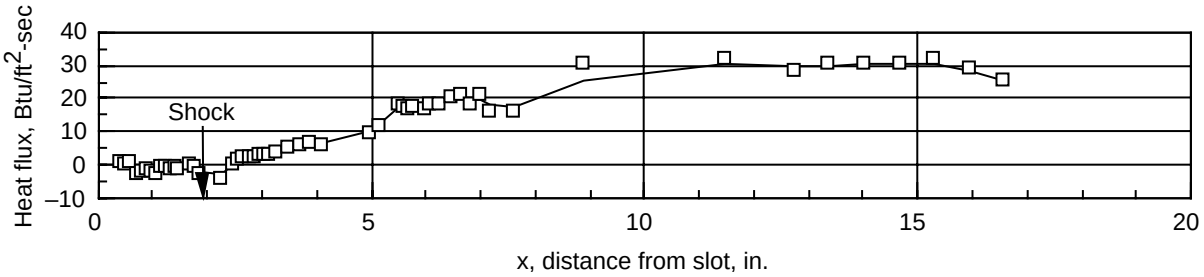

(b) 5.0° turning angle shock.

Figure 16. Incident-shock heat-flux distributions with hydrogen coolant at $m_c = 0.260$ ($p_c/p_e = 1.0$) and $R = 11.75 \times 10^6$.

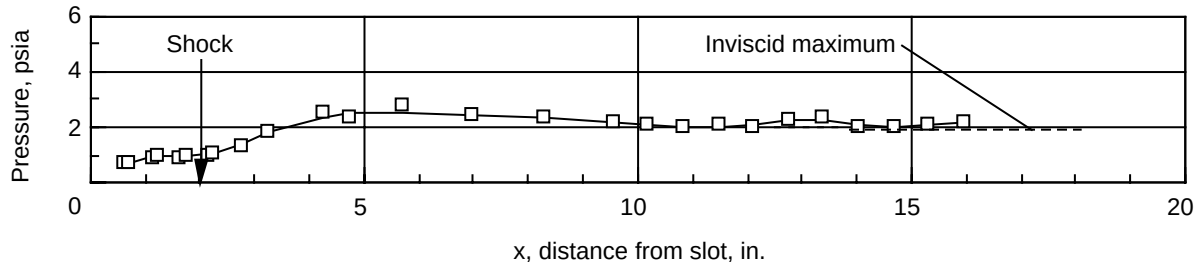

(a) 2.5° turning angle shock.

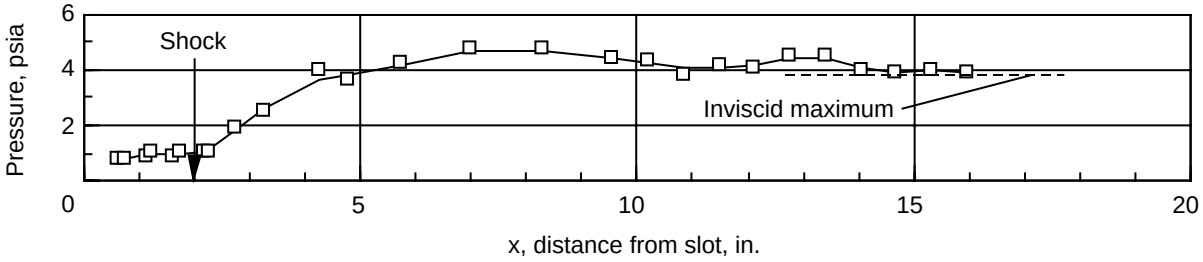

(b) 5.0° turning angle shock.

Figure 17. Incident-shock strength pressure distributions with hydrogen coolant at $m_c = 0.260$ ($p_c/p_e = 1.0$) and $R = 11.75 \times 10^6$.

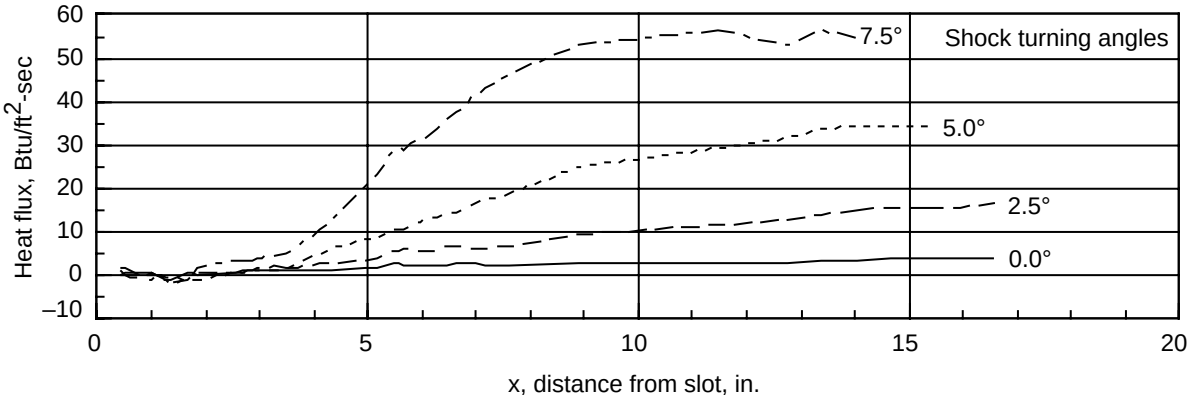

(a) Heat flux.

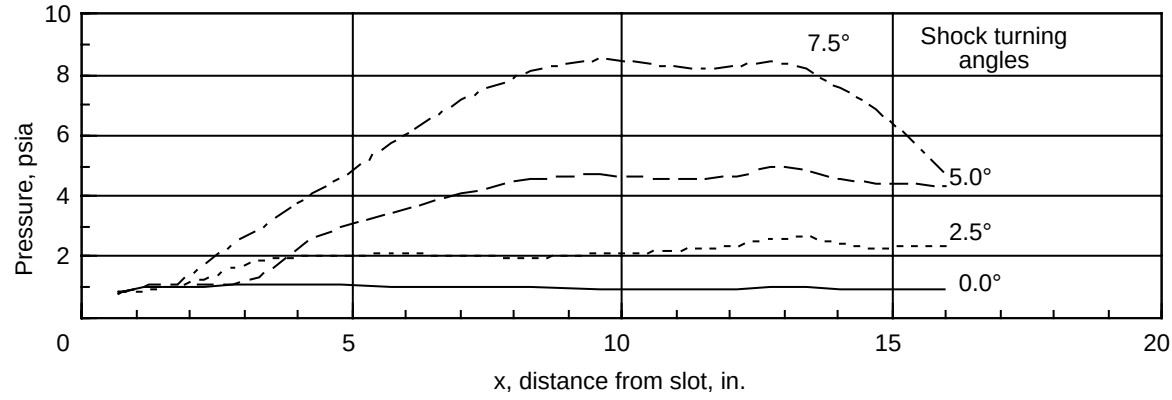

(b) Pressure.

Figure 18. Comparison of distributions for incident shock with hydrogen coolant at $m_c = 0.260$ ($p_c/p_e = 1.0$) and $R = 19.8 \times 10^6$.

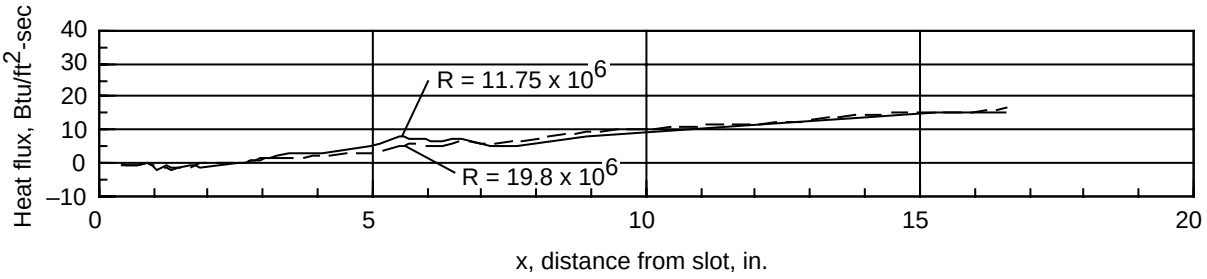

(a) 2.5° turning angle shock.

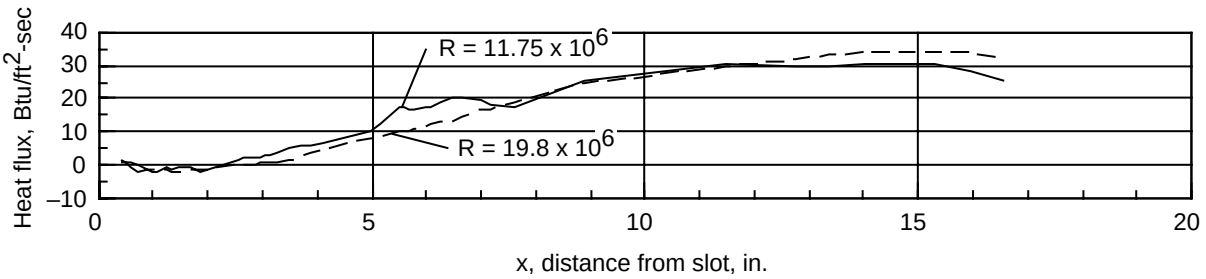

(b) 5.0° turning angle shock.

Figure 19. Comparison of heat-flux distributions with hydrogen coolant at $m_c = 0.260$ ($p_c/p_e = 1.0$) and $R = 11.75 \times 10^6$ and 19.8×10^6.

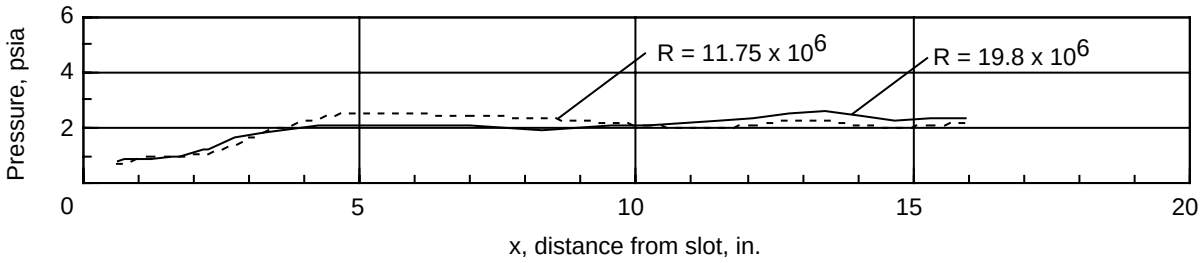

(a) 2.5° turning angle shock.

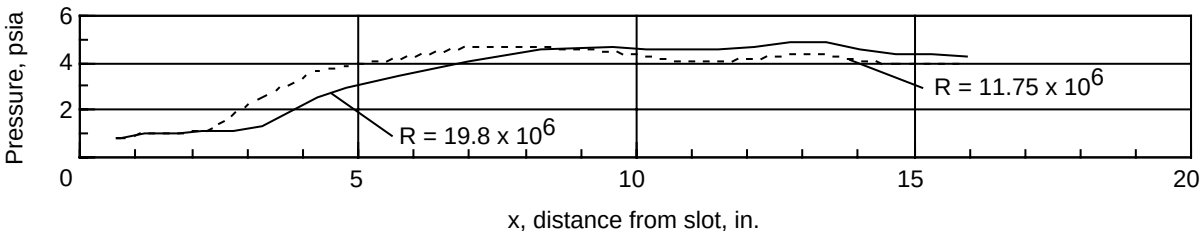

(b) 5.0° turning angle shock.

Figure 20. Comparison of pressure distribution data with hydrogen coolant at $m_c = 0.260$ ($p_c/p_e = 1.0$) and $R = 11.75 \times 10^6$ and 19.8×10^6.

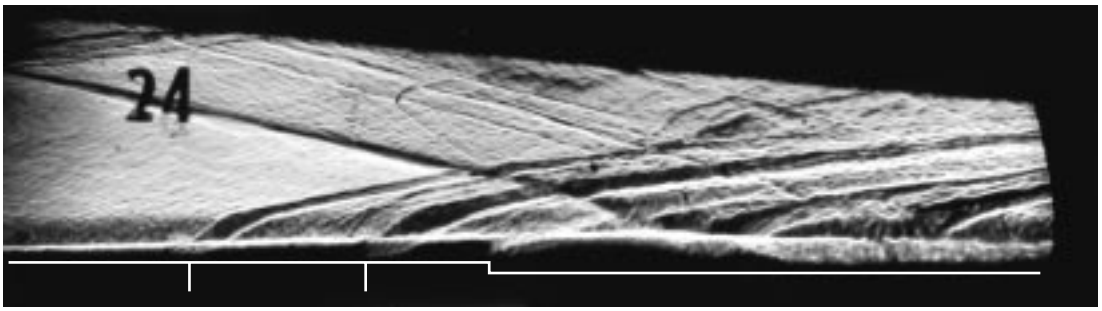

(a) Schlieren photograph.

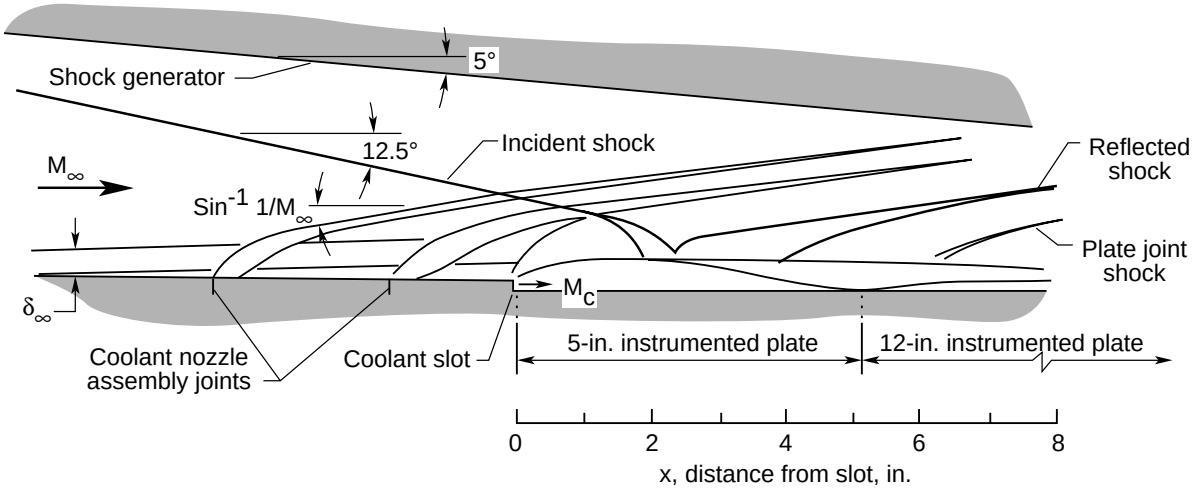

(b) Schematic.

Figure 21. Flow-field visualization for 5.0° incident shock with $R_{\infty} = 11.75 \times 10^6$ and hydrogen coolant at $p_c/p_e = 1.0$.

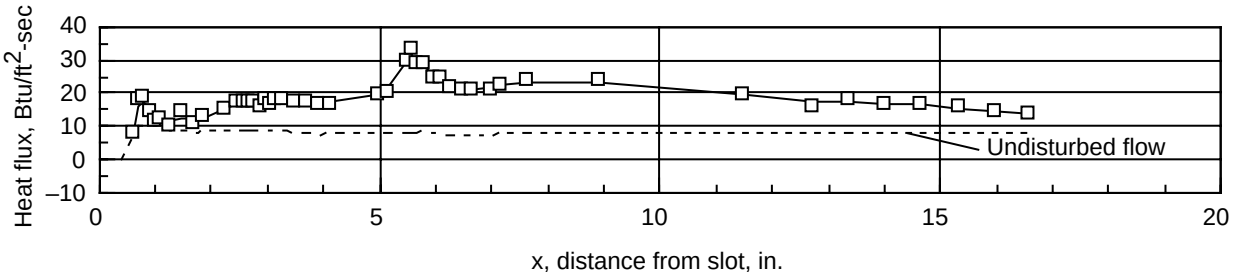

(a) Position 1 (y = –0.424 in.).

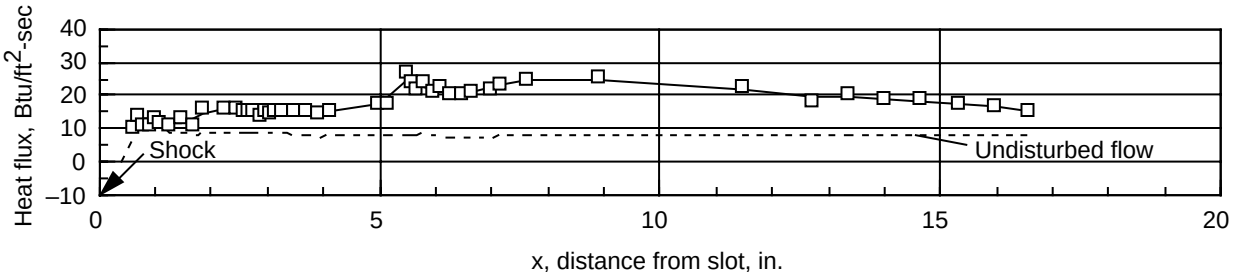

(b) Position 2 (y = 0.0 in.).

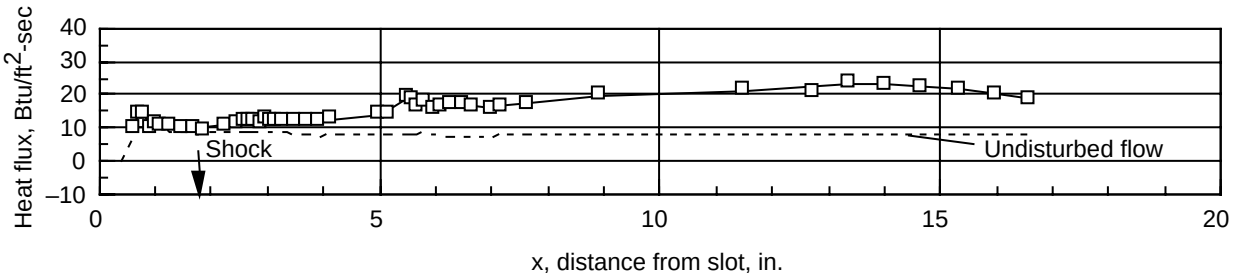

(c) Position 3 (y = 0.424 in.).

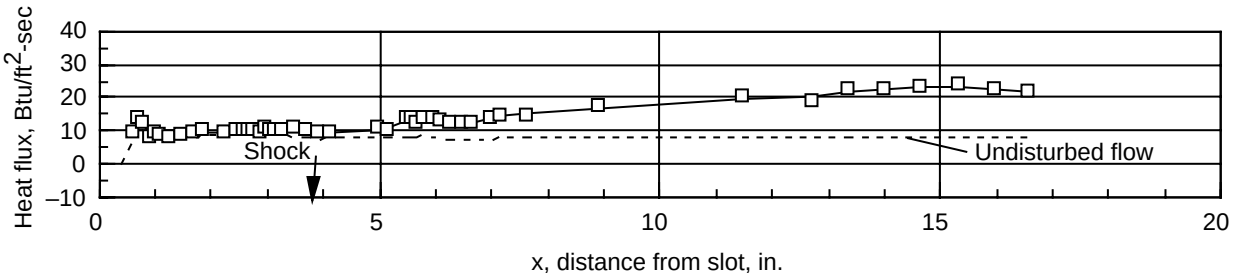

(d) Position 4 (y = 0.848 in.).

Figure 22. Heat-flux distribution for 5° swept shock with no coolant.

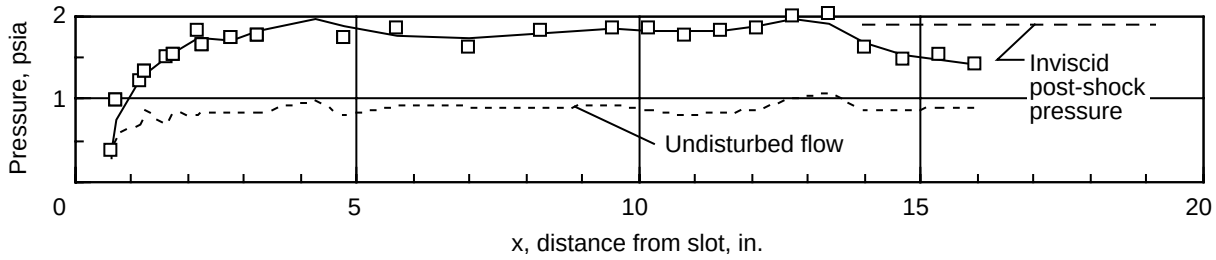

(a) Position 1 (y = –0.424 in.).

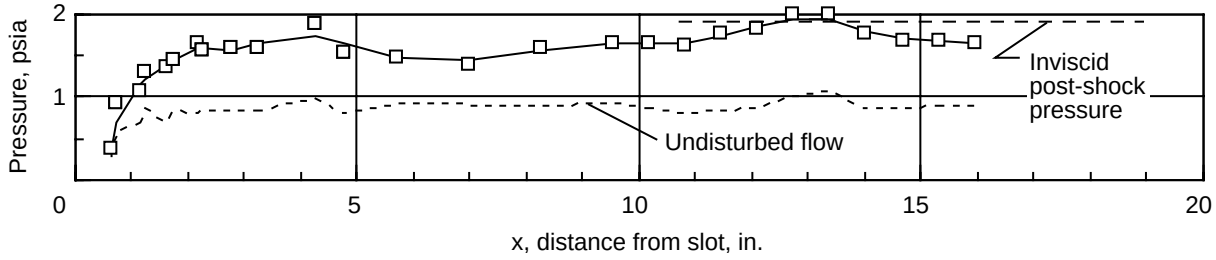

(b) Position 2 (y = 0.0 in.).

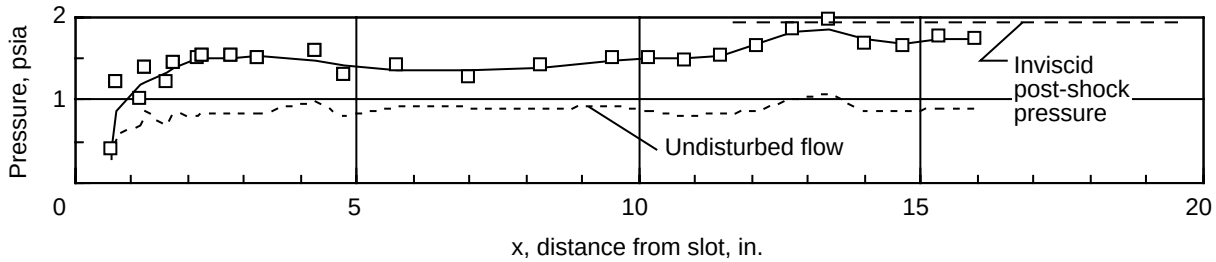

(c) Position 3 (y = 0.424 in.).

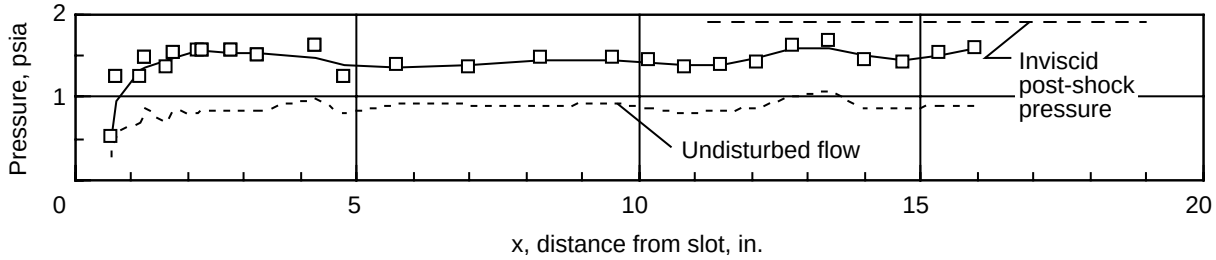

(d) Position 4 (y = 0.848 in.).

Figure 23. Pressure distribution for 5° swept shock with no coolant. (See fig. 5 for shock-instrumentation intersections.)

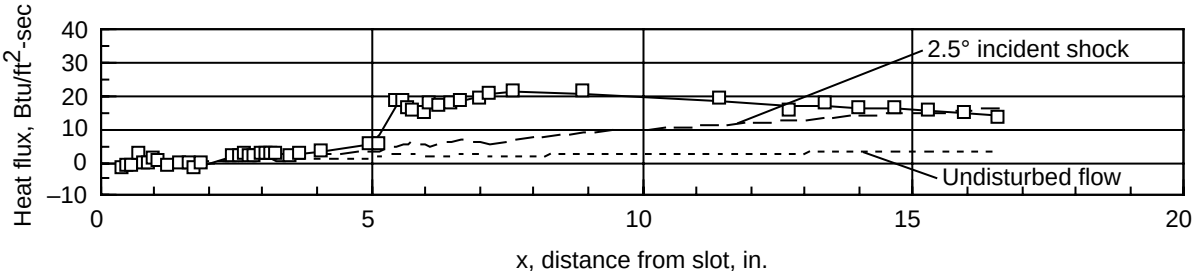

(a) Position 1 (y = –0.424 in.).

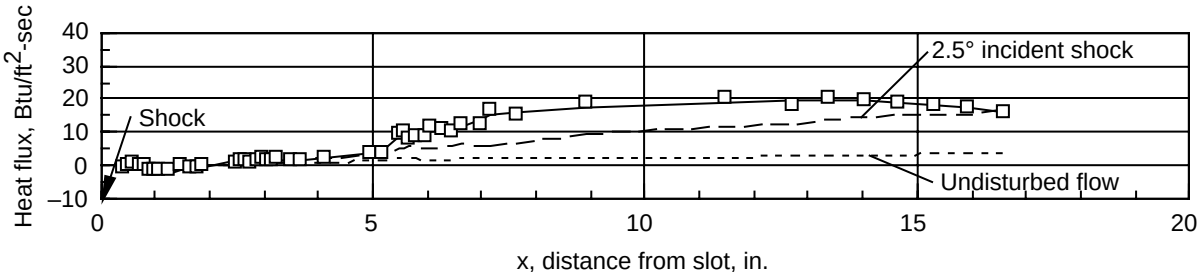

(b) Position 2 (y = 0.0 in.).

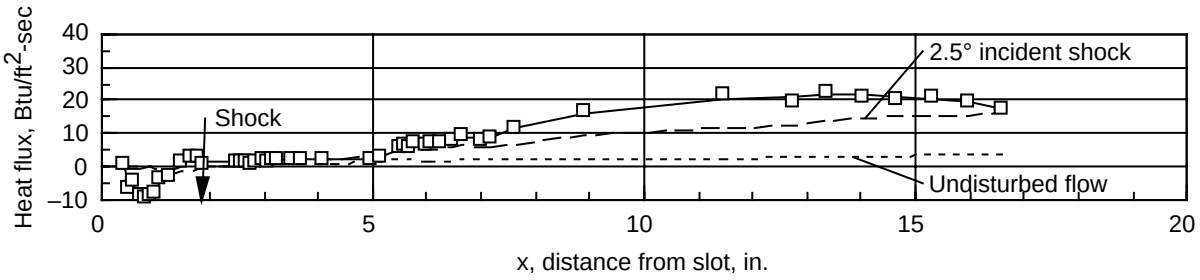

(c) Position 3 (y = 0.424 in.).

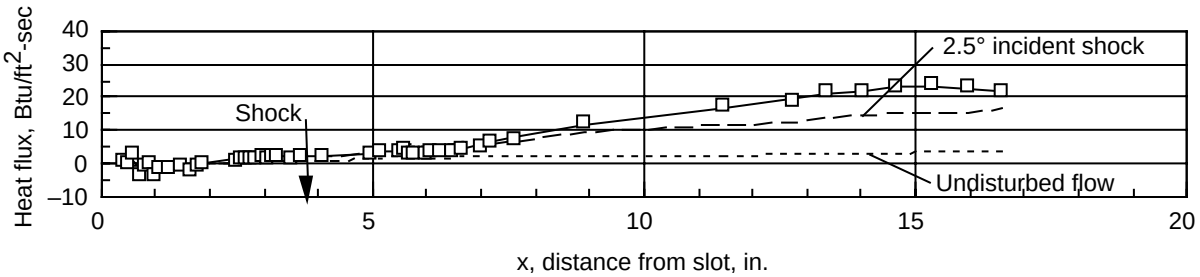

(d) Position 4 (y = 0.848 in.).

Figure 24. Heat-flux distribution for 5° swept shock with hydrogen coolant at m_c = 0.260 (p_c/p_e = 1.0).

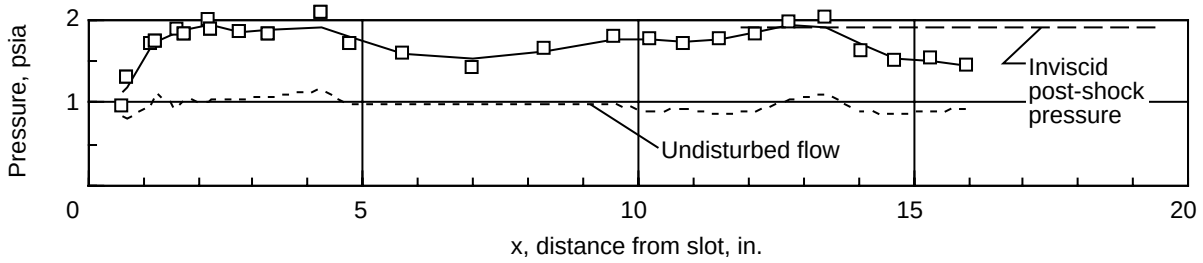

(a) Position 1 (y = –0.424 in.).

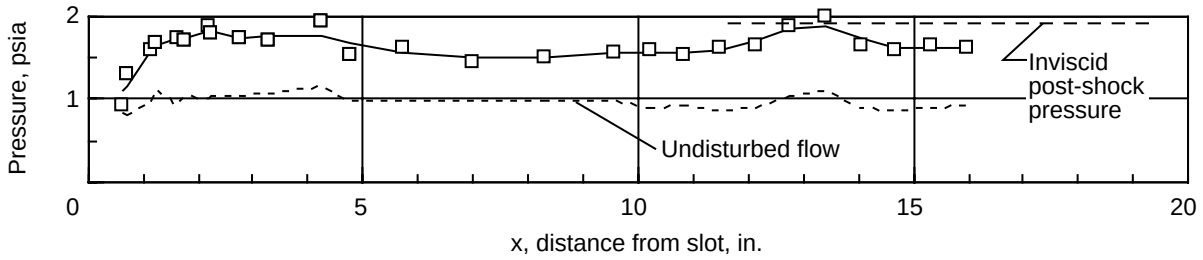

(b) Position 2 (y = 0.0 in.).

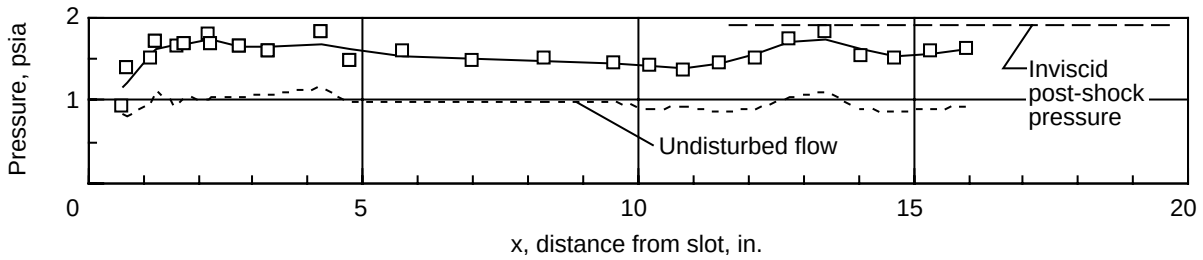

(c) Position 3 (y = 0.424 in.).

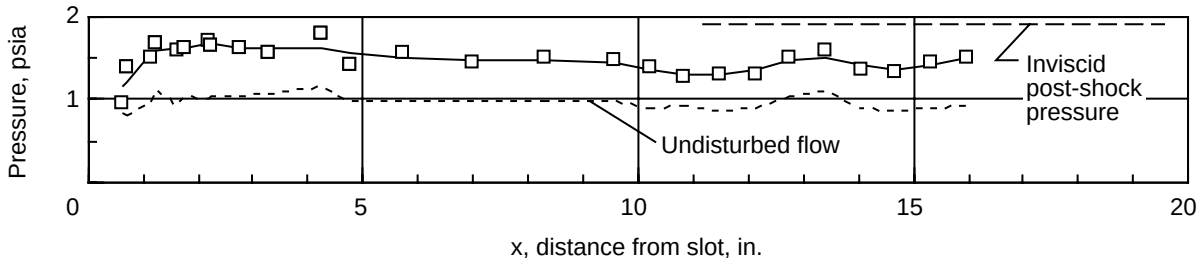

(d) Position 4 (y = 0.848 in.).

Figure 25. Pressure distribution for 5° swept shock with hydrogen coolant at m_c = 0.260 (p_c/p_e = 1.0). (See fig. 5 for shock-instrumentation intersections.)

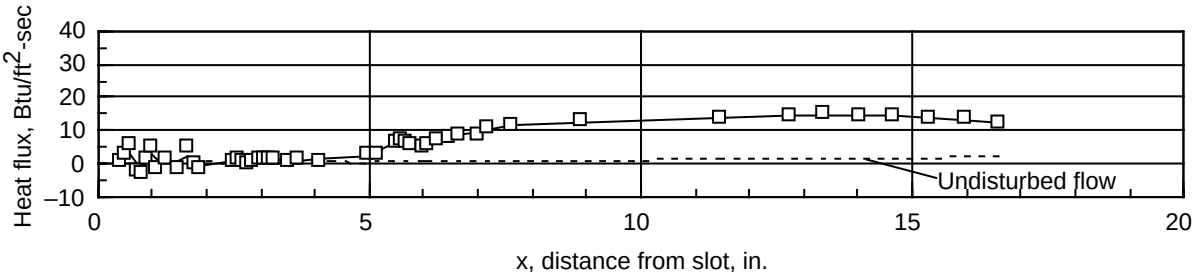

(a) Position 1 (y = –0.424 in.).

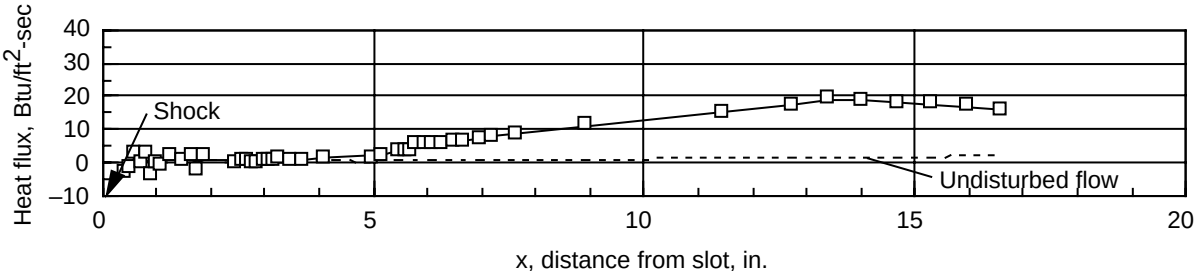

(b) Position 2 (y = 0.0 in.).

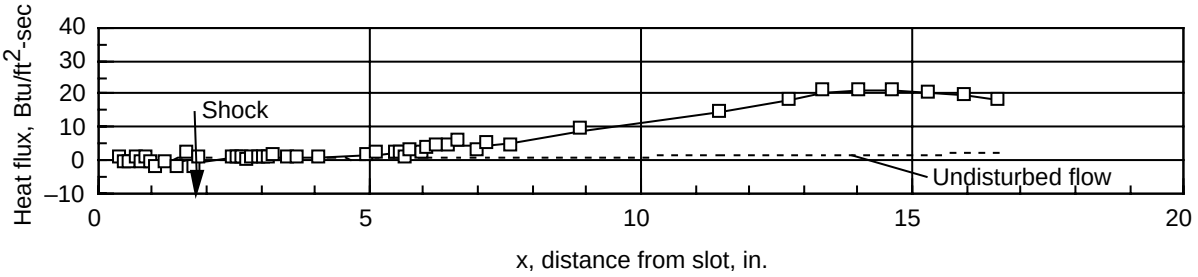

(c) Position 3 (y = 0.424 in.).

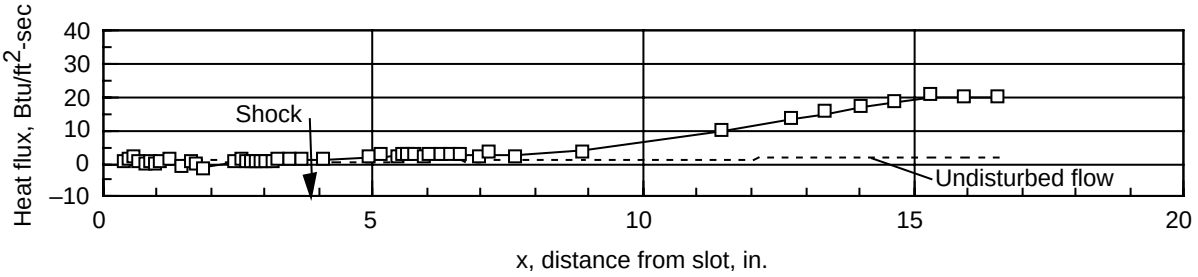

(d) Position 4 (y = 0.848 in.).

Figure 26. Heat-flux distribution for 5° swept shock with hydrogen coolant at m_c = 0.662 (p_c/p_e = 2.0).

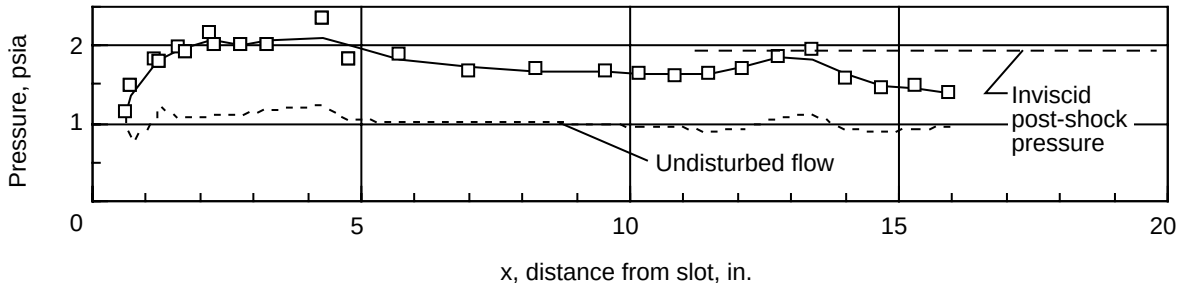

(a) Position 1 (y = –0.424 in.).

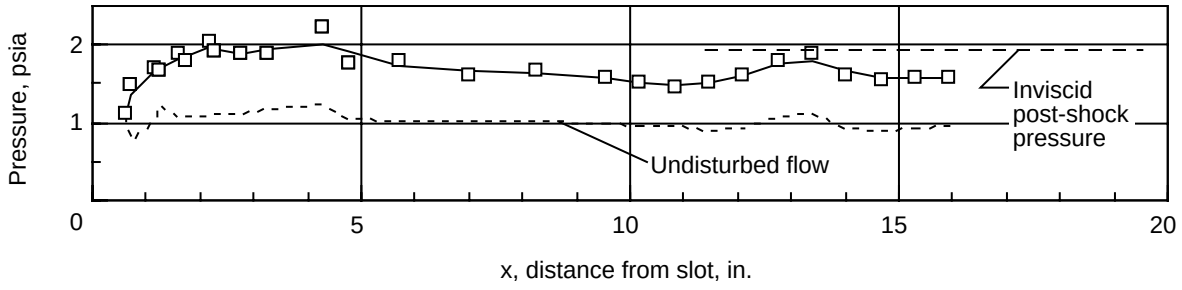

(b) Position 2 (y = 0.0 in.).

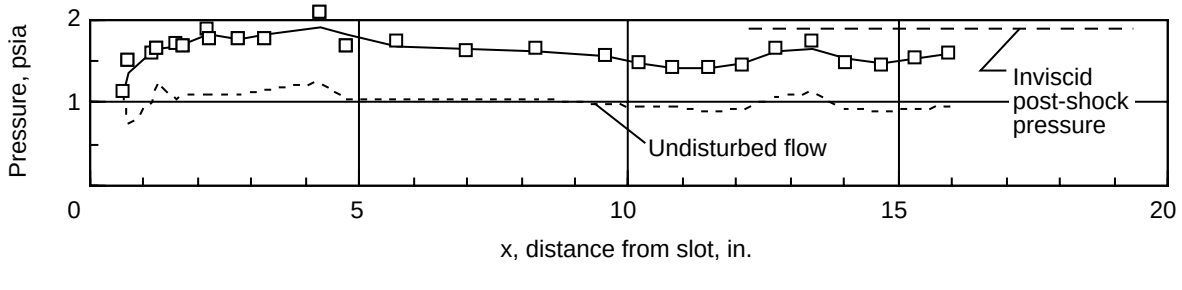

(c) Position 3 (y = 0.424 in.).

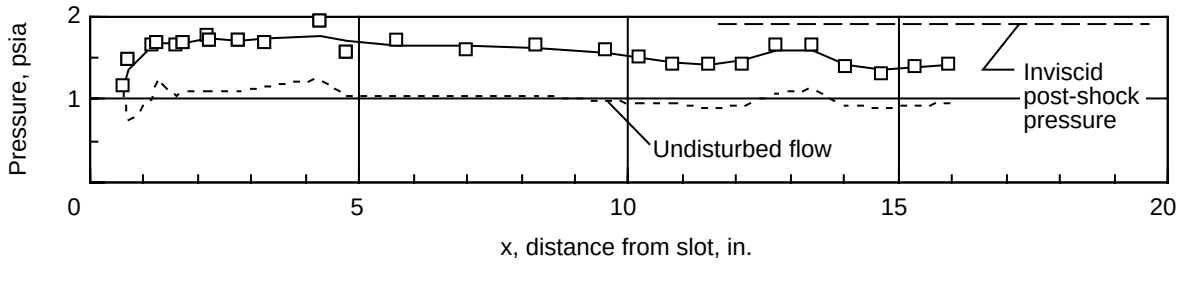

(d) Position 4 (y = 0.848 in.).

Figure 27. Pressure distribution for 5° swept shock with hydrogen coolant at m_c = 0.660 (p_c/p_e = 2.0). (See fig. 5 for shock-instrumentation intersections.)

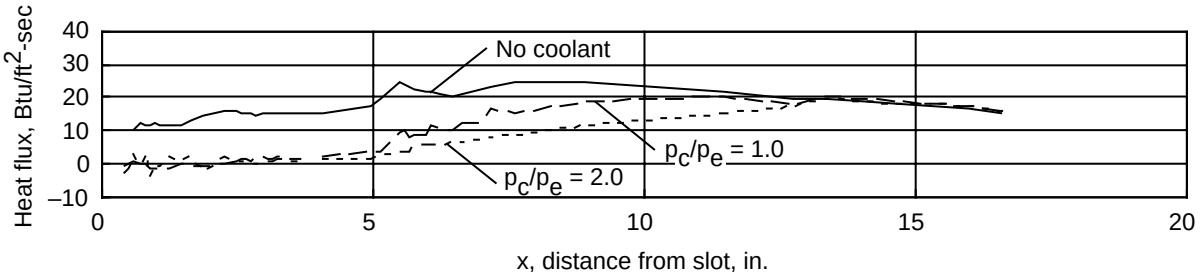

(a) Heat flux.

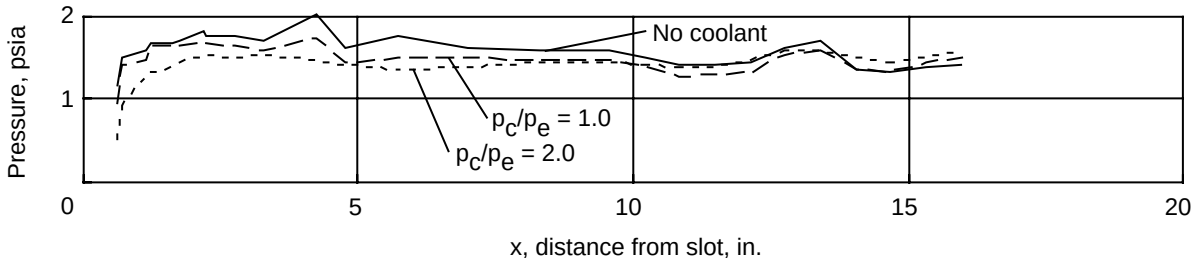

(b) Pressure.

Figure 28. Composite of heat-flux and pressure coincident data at equivalent shock location. y = 0.0 in.

REPORT DOCUMENTATION PAGE

Form Approved
OMB No. 0704-0188

1. AGENCY USE ONLY *(Leave blank)*	2. REPORT DATE	3. REPORT TYPE AND DATES COVERED
	June 1995	Technical Memorandum

4. TITLE AND SUBTITLE
Hydrogen Film Cooling With Incident and Swept-Shock Interactions in a Mach 6.4 Nitrogen Free Stream

5. FUNDING NUMBERS
WU 506-43-31-03

6. AUTHOR(S)
George C. Olsen and Robert J. Nowak

7. PERFORMING ORGANIZATION NAME(S) AND ADDRESS(ES)
NASA Langley Research Center
Hampton, VA 23681-0001

8. PERFORMING ORGANIZATION REPORT NUMBER
L-17367

9. SPONSORING/MONITORING AGENCY NAME(S) AND ADDRESS(ES)
National Aeronautics and Space Administration
Washington, DC 20546-0001

10. SPONSORING/MONITORING AGENCY REPORT NUMBER
NASA TM-4603

11. SUPPLEMENTARY NOTES

12a. DISTRIBUTION/AVAILABILITY STATEMENT
Unclassified–Unlimited
Subject Category 34
Availability: NASA CASI (301) 621-0390

12b. DISTRIBUTION CODE

13. ABSTRACT *(Maximum 200 words)*
The effectiveness of slot film cooling of a flat plate in a Mach 6.4 flow with and without incident and swept oblique shock interactions was experimentally investigated. Hydrogen was the primary coolant gas, although some tests were conducted using helium as the coolant. Tests were conducted in the Calspan 48-Inch Shock Tunnel with a nitrogen flow field to preclude combustion of the hydrogen coolant gas. A two-dimensional highly instrumented model developed in a previous test series was used. Parameters investigated included coolant mass flow rate, coolant gas, local free-stream Reynolds number, incident oblique shock strength, and a swept oblique shock. Both gases were highly effective coolants in undisturbed flow; however, both incident and swept shocks degraded that effectiveness.

14. SUBJECT TERMS
Film cooling; Heat transfer data; Shock interactions; Pressure data

15. NUMBER OF PAGES
45

16. PRICE CODE
A03

17. SECURITY CLASSIFICATION OF REPORT	18. SECURITY CLASSIFICATION OF THIS PAGE	19. SECURITY CLASSIFICATION OF ABSTRACT	20. LIMITATION OF ABSTRACT
Unclassified	Unclassified	Unclassified	